



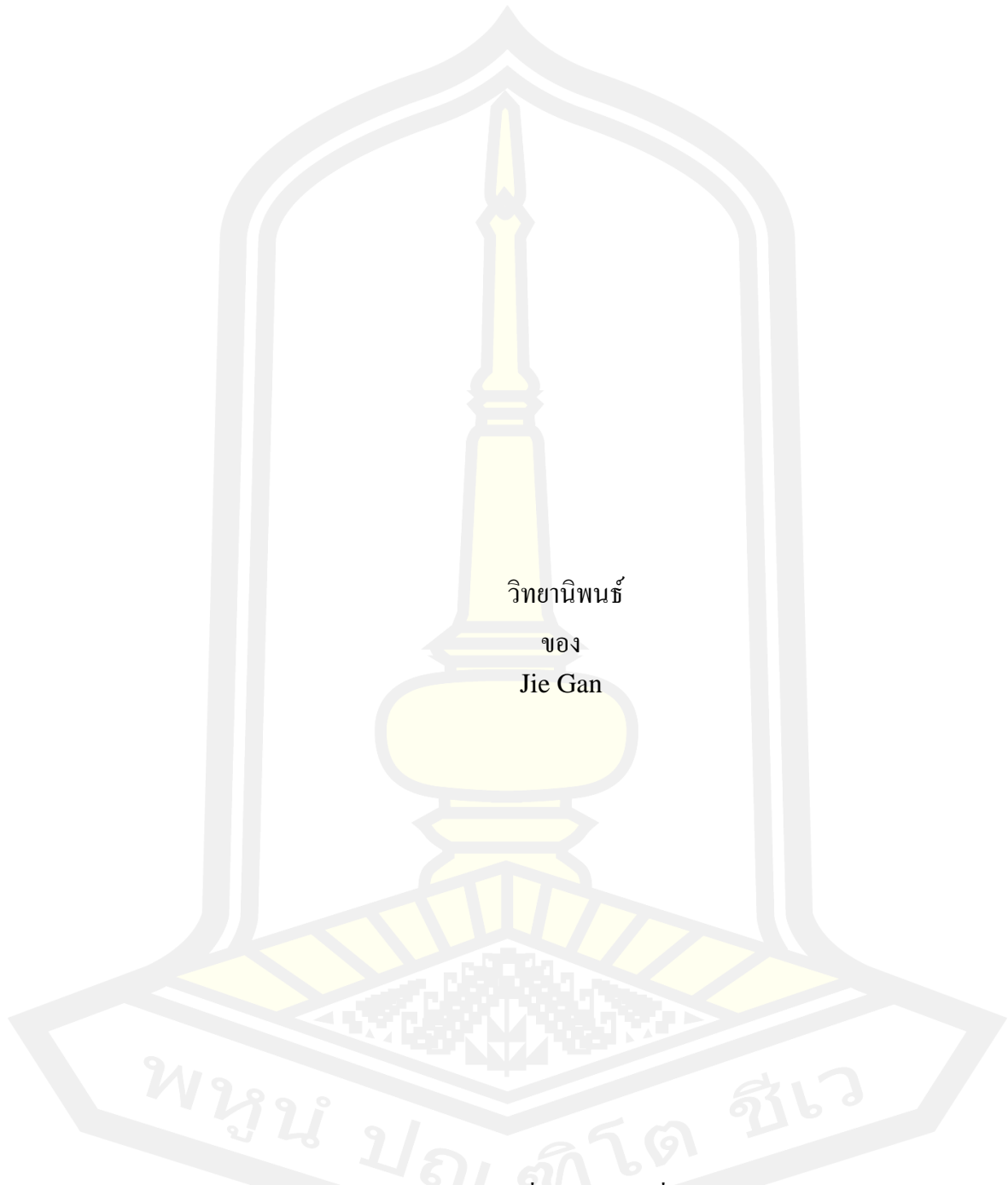
# GaN Based Robot Power Supply Design

Jie Gan

A Thesis Submitted in Partial Fulfillment of Requirements for  
degree of Master of Engineering in Electrical and Computer Engineering  
September 2022

Copyright of Mahasarakham University

การออกแบบแหล่งจ่ายไฟฟ้าด้วยอุปกรณ์แกเลียมไนเตรท

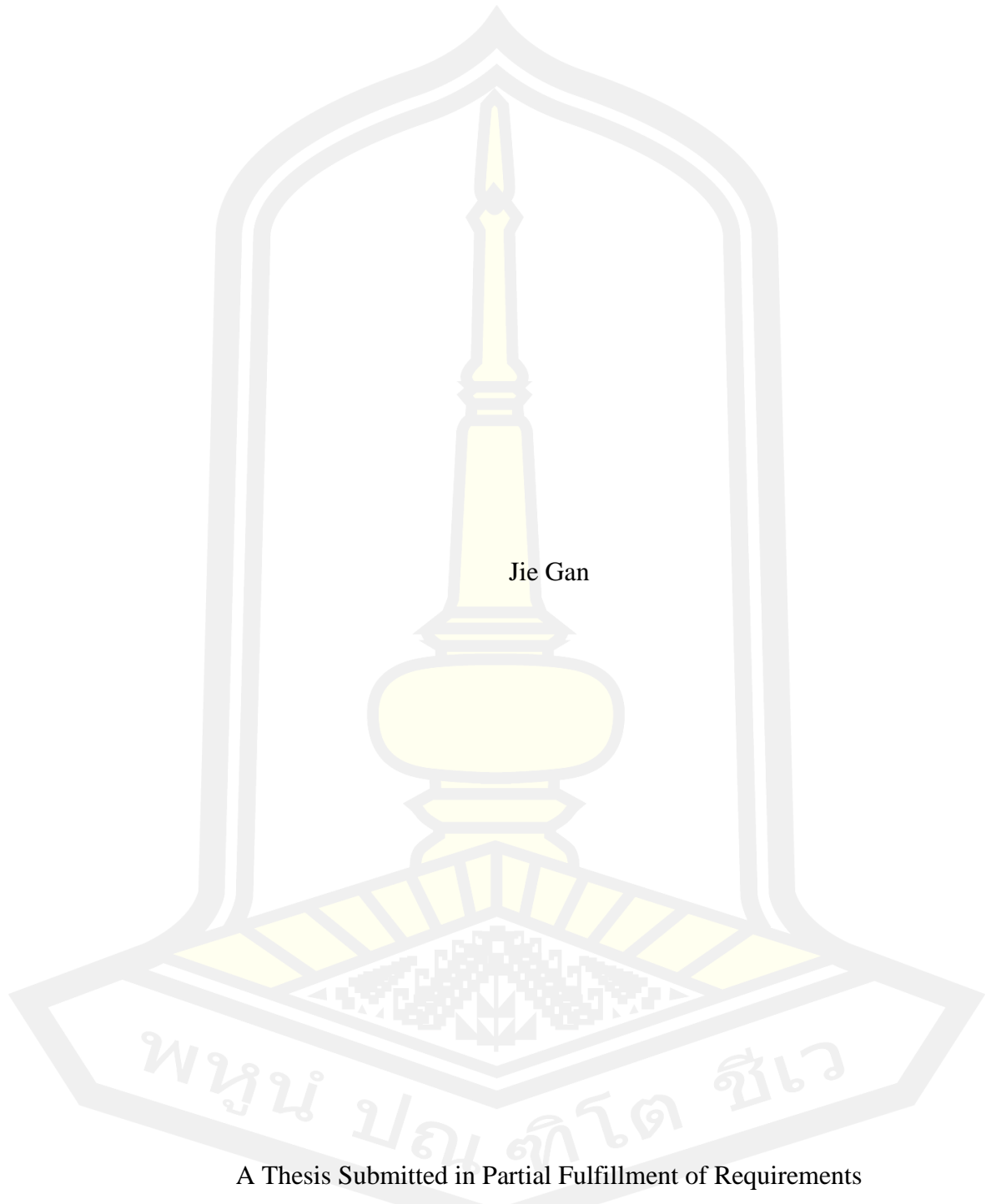


เสนอต่อมหาวิทยาลัยมหาสารคาม เพื่อเป็นส่วนหนึ่งของการศึกษาตามหลักสูตร  
ปริญญาวิทยาศาสตรมหาบัณฑิต สาขาวิชาวิศวกรรมไฟฟ้าและคอมพิวเตอร์

กันยายน 2565

ลิขสิทธิ์เป็นของมหาวิทยาลัยมหาสารคาม

# GaN Based Robot Power Supply Design



Jie Gan

A Thesis Submitted in Partial Fulfillment of Requirements  
for Master of Engineering (Electrical and Computer Engineering)

September 2022

Copyright of Mahasarakham University



The examining committee has unanimously approved this Thesis, submitted by Mr. Jie Gan , as a partial fulfillment of the requirements for the Master of Engineering Electrical and Computer Engineering at Maharakham University

Examining Committee

..... Chairman  
(Asst. Prof. Adirek Jantakun , Ph.D.)

..... Advisor  
(Assoc. Prof. Chonlatee Photong ,  
Ph.D.)

..... Committee  
(Asst. Prof. Supannika Wattana ,  
Ph.D.)

..... Committee  
(Asst. Prof. Niwat Angkawisittpan ,  
Ph.D.)

Maharakham University has granted approval to accept this Thesis as a partial fulfillment of the requirements for the Master of Engineering Electrical and Computer Engineering

..... (Assoc. Prof. Keartisak Sriprateep , (Assoc. Prof. Krit Chaimoon , Ph.D.)  
Ph.D.) Dean of Graduate School  
Dean of The Faculty of Engineering

**TITLE** GaN Based Robot Power Supply Design  
**AUTHOR** Jie Gan  
**ADVISORS** Associate Professor Chonlatee Photong , Ph.D.  
**DEGREE** Master of Engineering **MAJOR** Electrical and Computer Engineering  
**UNIVERSITY** Mahasarakham University **YEAR** 2022

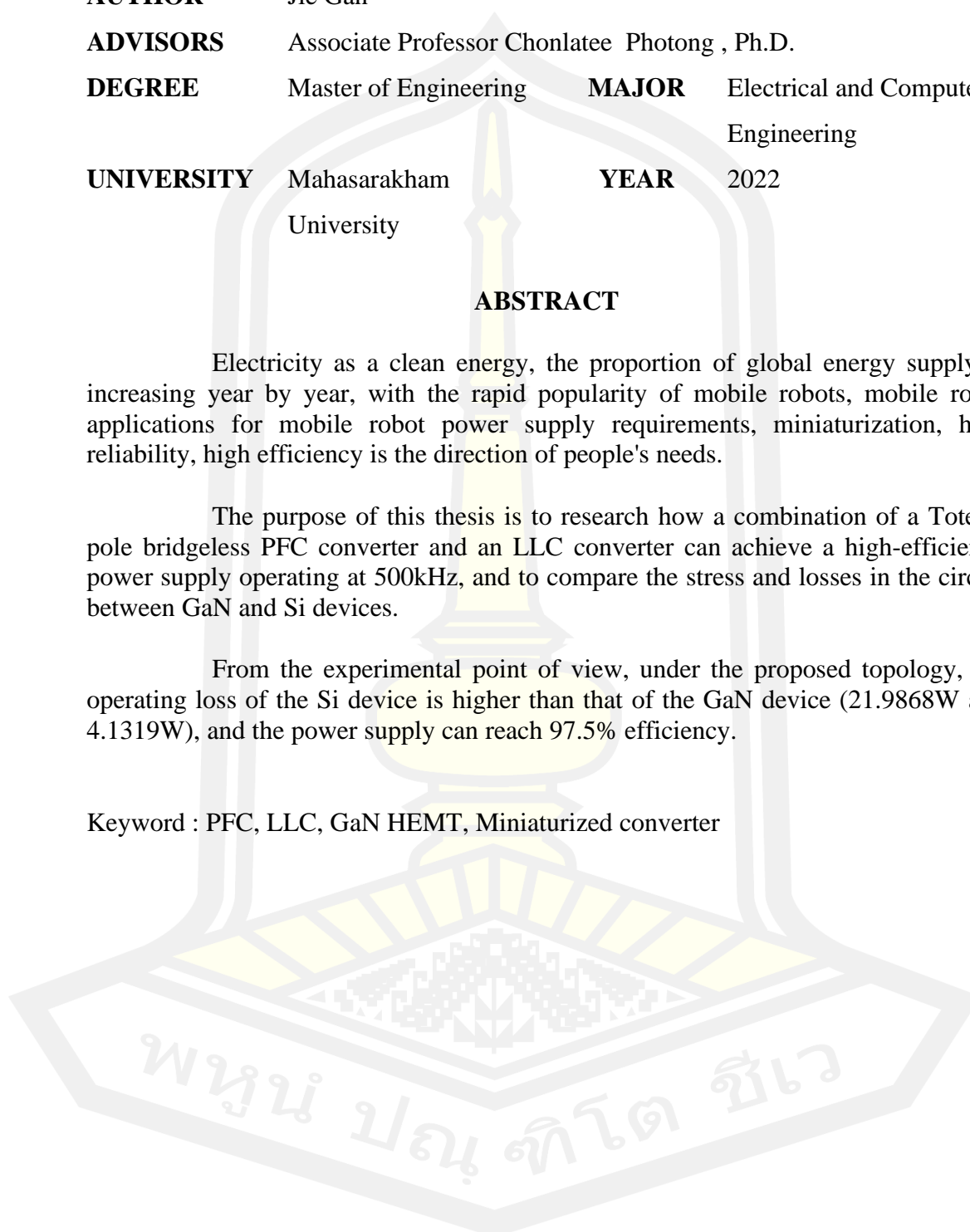
### ABSTRACT

Electricity as a clean energy, the proportion of global energy supply is increasing year by year, with the rapid popularity of mobile robots, mobile robot applications for mobile robot power supply requirements, miniaturization, high reliability, high efficiency is the direction of people's needs.

The purpose of this thesis is to research how a combination of a Totem-pole bridgeless PFC converter and an LLC converter can achieve a high-efficiency power supply operating at 500kHz, and to compare the stress and losses in the circuit between GaN and Si devices.

From the experimental point of view, under the proposed topology, the operating loss of the Si device is higher than that of the GaN device (21.9868W and 4.1319W), and the power supply can reach 97.5% efficiency.

Keyword : PFC, LLC, GaN HEMT, Miniaturized converter



## ACKNOWLEDGEMENTS

Time flies, and the two-year master study period is coming to an end. On the occasion of completing my dissertation, I would like to express my heartfelt thanks and deep respect to my supervisor Associate Professor Chonlatee Photong, Ph.D. My supervisor's profound academic attainments, pragmatic working style, rich practical experience and rigorous academic attitude have benefited me for the rest of my life. This thesis could not have been completed without the support of my supervisor.

As well as, I would like to thank all the examination boards who have provided me with a lot of advice and suggestions for writing my thesis. My sincere thanks to Maharakham University College of Engineering for facilitating my research.

In addition, I would like to thank to my parents and everyone who has supported and encouraged me during my study at Maharakham University, Thailand.

Jie Gan

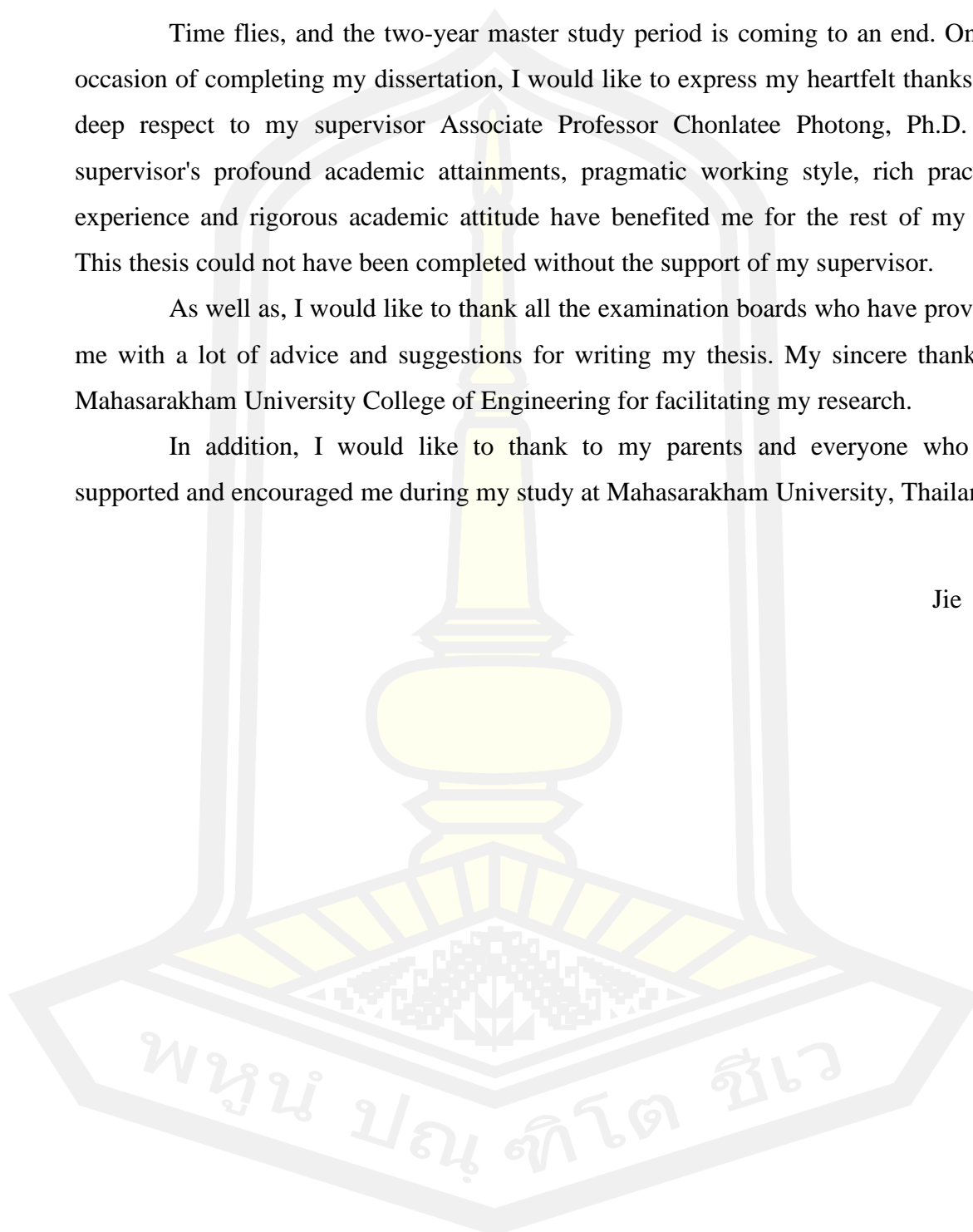


## TABLE OF CONTENTS

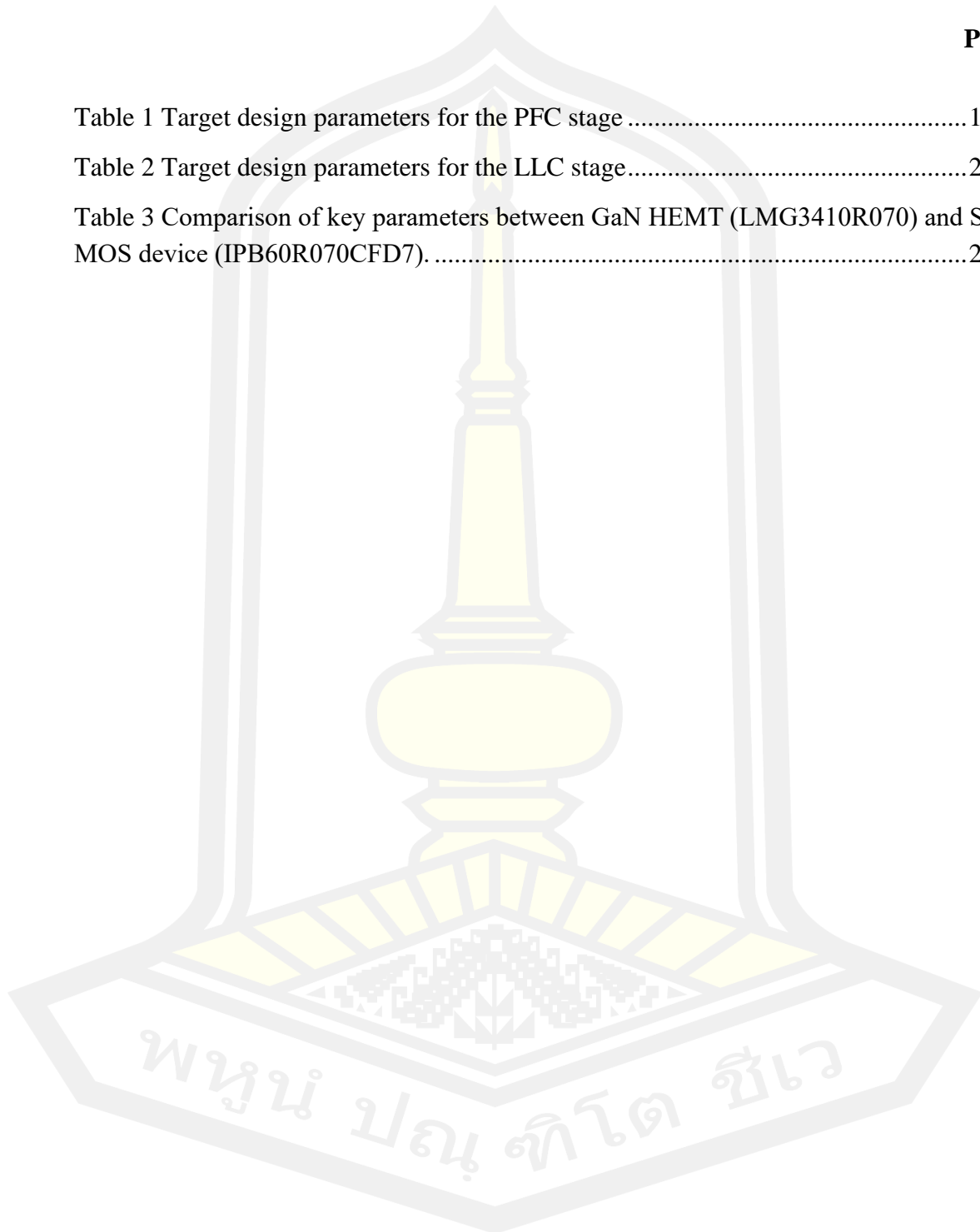
	<b>Page</b>
ABSTRACT.....	D
ACKNOWLEDGEMENTS.....	E
TABLE OF CONTENTS.....	F
LIST OF TABLES.....	H
LIST OF FIGURES.....	I
CHAPTER I.....	1
INTRODUCTION.....	1
Overview.....	1
1. Industrial robots.....	2
2. Service robots.....	2
3. Military robots.....	2
4. Medical robots.....	2
5. Simulation robots.....	3
Charging modes for mobile robots.....	4
1. Conventional charging mode.....	4
2. Fast charging mode.....	4
3. Battery replacement method.....	4
Project Importance.....	5
Purposes of Research.....	5
CHAPTER II.....	6
LITERATURE REVIEW.....	6
AC-DC.....	6
DC-DC.....	8
Control Strategy.....	10
1. Boost PFC circuit control strategy.....	10

2. LLC resonant converter control strategy .....	10
Power supply complete topology .....	11
Selection of semiconductor devices .....	11
CHAPTER III .....	13
METHODOLOGY .....	13
Totem-pole bridgeless PFC control logic .....	13
Design of the Totem-pole bridgeless PFC Converter Parameters .....	14
LLC resonant converter control logic .....	16
1. How it works when $f_m < f < f_s$ .....	16
2. How it works when $f = f_s$ .....	20
3. How it works when $f > f_s$ .....	21
Design of the LLC Resonant Converter Parameters .....	25
CHAPTER IV .....	28
TEST RESULTS AND DISCUSSIONS .....	28
Simulation Models .....	28
Simulated Results .....	29
1. Comparison of the Outputs .....	30
2. Comparison of Voltage and Current Stresses on Semiconductor Devices ...	31
3. Semiconductor device loss comparison .....	33
CHAPTER V .....	36
CONCLUSIONS .....	36
Conclusions .....	36
Suggestions and Future Works .....	37
REFERENCES .....	38
BIOGRAPHY .....	43



**LIST OF TABLES**

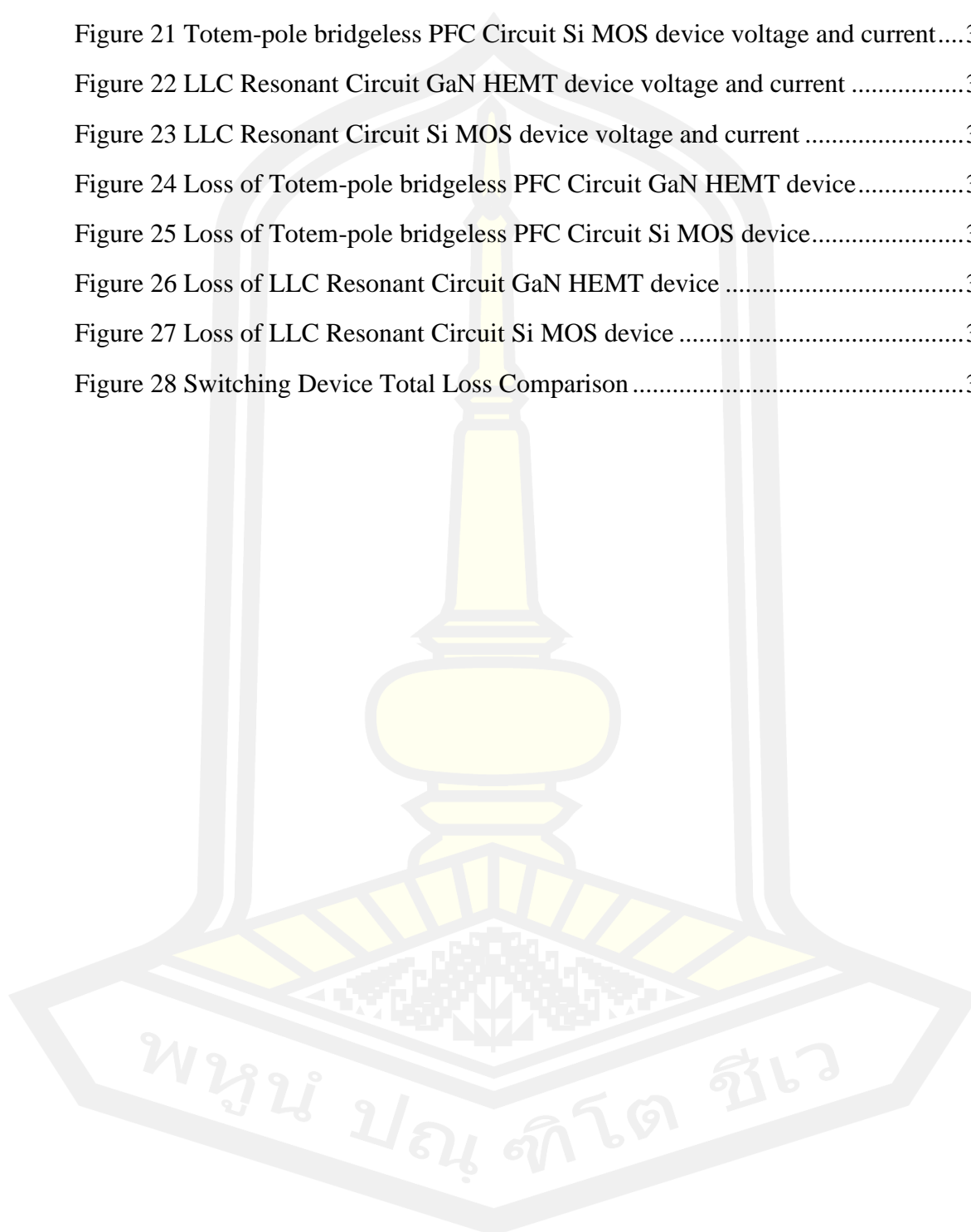
	<b>Page</b>
Table 1 Target design parameters for the PFC stage .....	14
Table 2 Target design parameters for the LLC stage.....	25
Table 3 Comparison of key parameters between GaN HEMT (LMG3410R070) and Si MOS device (IPB60R070CFD7). .....	29



## LIST OF FIGURES

	<b>Page</b>
Figure 1 robot classification [3].....	1
Figure 2 TOP 5 applications for professional use [5].....	3
Figure 3 PFC converters (a) Diode bridge converter [22], (b) Symmetrical bridgeless [23], (c) Symmetrical bridgeless with common mode filter [24], (d) Two-way switch bridgeless PFC [15], (e) totem-pole bridgeless [25], (f) Fake Totem Pole PFC .....	7
Figure 4 LLC converter topology [25].....	9
Figure 5 The converter configuration of the proposed system. ....	11
Figure 6 Summary of Si, SiC, and GaN relevant material properties [49].....	12
Figure 7 Totem-pole bridgeless PFC simplified illustration [17].....	13
Figure 8 LLC resonant circuit Operation sequence with $f_m < f < f_s$ .....	18
Figure 9 LLC resonant circuit Operation waveforms with $f_m < f < f_s$ .....	18
Figure 10 LLC resonant circuit Operation waveforms with $f = f_s$ .....	21
Figure 11 LLC resonant circuit Operation sequence with $f > f_s$ .....	24
Figure 12 LLC resonant circuit Operation waveforms with $f > f_s$ .....	24
Figure 13 Totem-pole bridgeless PFC Simulation Circuit .....	28
Figure 14 LLC Simulation Circuit.....	28
Figure 15 simulation schematic diagram details comparison, (1) GaN HEMT (LMG3410R070), (2) Si MOS (IPB60R070CFD7) .....	29
Figure 16 Totem-pole bridgeless PFC Circuit output voltage and current waveforms using the GaN HEMT device.....	30
Figure 17 Totem-pole bridgeless PFC Circuit output voltage and current waveform using the Si MOS device .....	30
Figure 18 LLC Resonant Circuit output voltage and current waveform using the GaN HEMT device.....	31
Figure 19 LLC Resonant Circuit output voltage and current waveform using the Si MOS device .....	31

Figure 20 Totem-pole bridgeless PFC Circuit GaN HEMT device voltage and current .....	32
Figure 21 Totem-pole bridgeless PFC Circuit Si MOS device voltage and current....	32
Figure 22 LLC Resonant Circuit GaN HEMT device voltage and current .....	33
Figure 23 LLC Resonant Circuit Si MOS device voltage and current .....	33
Figure 24 Loss of Totem-pole bridgeless PFC Circuit GaN HEMT device.....	34
Figure 25 Loss of Totem-pole bridgeless PFC Circuit Si MOS device.....	34
Figure 26 Loss of LLC Resonant Circuit GaN HEMT device .....	35
Figure 27 Loss of LLC Resonant Circuit Si MOS device .....	35
Figure 28 Switching Device Total Loss Comparison .....	36



# CHAPTER I

## INTRODUCTION

### Overview

There are a number of robots increasing nowadays due to the fast growth of Artificial Intelligent (AI) that has improved many operations of machines and is widely adopted in industries such as medical, healthcare, service, hospitality, and manufacturing. This is because of the fact that these robots and machines have been employed to perform humans operations during this industrial revolution worldwide [1].

With the development of the robot industry, the scope of applications of robots is no longer limited to the industrial field and direction of service fields, such as cleaning robots, early education robots, entertainment robots, and guiding robots. There are also some robots used in special environments and occasions, such as disaster relief robots, defense robots, and detection robots. In addition, more and more bionic robots are being developed and applied, such as bionic pet dogs. Therefore the applications of robots seem to be one of the most attractive study fields for many researchers worldwide.

In general, the service robots are classified into two types by the International Federation of Robotics (IFR): Personal/household service robots and specialist service robots [2] as shown in Figure 1.

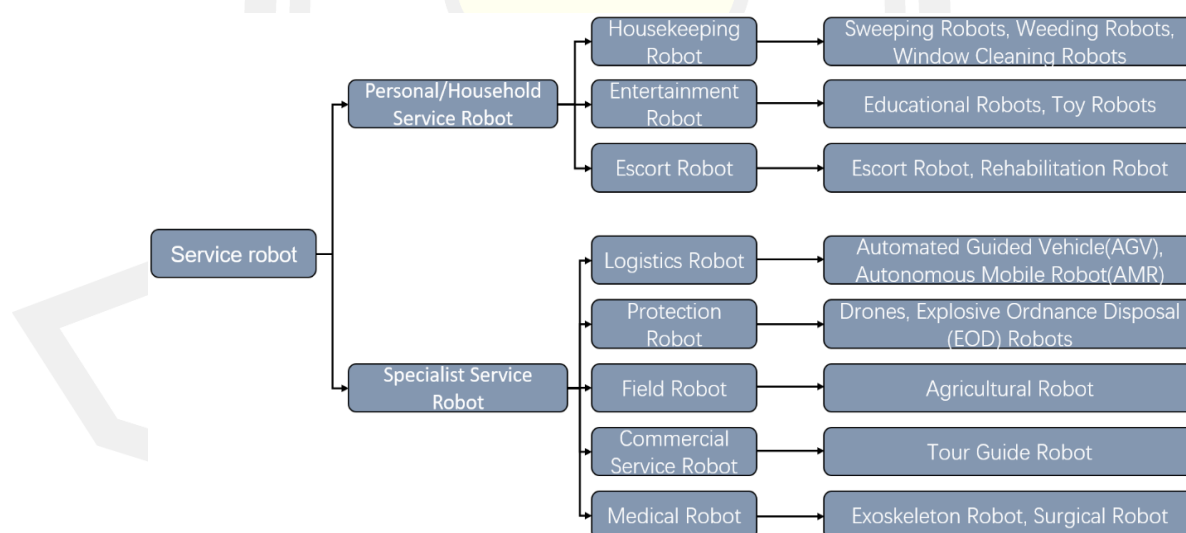


**Figure 1** robot classification [3]

Alternatively, the robots could be classified as listed in the following categories:

## **1. Industrial robots**

Industrial robots are important automation equipment in modern manufacturing that integrates advanced technologies such as machinery, electronics, control, computers, sensors, and artificial intelligence. After more than 50 years of development, industrial robots have been applied in more and more fields. In the manufacturing industry, especially in the automotive industry, industrial robots have been widely used.

The practice has proved that industrial robots are very suitable for heavy work, simple repetitive work, dangerous work, and work in harsh environments (high temperature, flammable, explosive, toxic, corrosive, etc.), which can effectively ensure labor safety and prevent occupational diseases. Improve the labor environment and greatly increase labor productivity. In addition, the introduction of industrial robots contributes to product quality and reliability.

## **2. Service robots**

Service robots are a kind of semi-autonomous or fully autonomous robots, which can complete the service work that is beneficial to human beings. This kind of robot is mainly used in the service industry, such as cleaning robots, entertainment, and education robots, rehabilitation robots, and nursing robots for the elderly and the disabled.

## **3. Military robots**

Military robots are robotic systems designed and developed to perform various military tasks. From unmanned combat vehicles to small automatic devices like reptiles, military robots are an important combat force that cannot be ignored on the battlefield despite their diverse forms. With the development of technology, more and more robots will appear in various places that are more dangerous or unsuitable for people to reach.

In the field of military robots, the United States is a well-deserved world hegemon. On the battlefields of Afghanistan and Iraq, various military robots of the US military have been used for large-scale verification. In recent years, the focus of the US military's military robot research and development has been shifting from auxiliary equipment to main combat readiness. The emergence of unmanned intelligent combat aircraft represented by X-47B is a representative of this trend.

## **4. Medical robots**

Medical robots are currently mainly used in medical surgical planning simulation, micro-damage precise positioning operation, non-damage diagnosis and detection, new surgical medical treatment methods, etc. The emergence of medical robots not only promoted the revolution of traditional medicine but also led to the development of new technologies and new theories.

## 5. Simulation robots

Simulation robots, as the name suggests, are robots that can imitate humans, and they can be called the "Pearl in the Crown" in the field of robotics. In this field, Japan has the most prominent technological advantage.

Commercial, high-tech and social driving factors have had an accelerating effect on mobile robots, especially autonomous mobile robots. By 2025, the market penetration rate of mobile robots will still not exceed 30%, but the market opportunities for autonomous guided vehicles and autonomous mobile robots are still unprecedentedly huge. Especially the warehousing industry will become a huge market for mobile robot suppliers. According to research and analysis, 2020 marked a watershed in the industry. As the economy resumes growth in the middle of the year, it was reported that the total shipments of mobile robots in 2020 would increase by more than 25%, and nearly 60,000 AGVs and AMRs will be deployed [4].

The professional service robot market will grow 12% in 2020, from \$6 billion to \$6.7 billion. Global robotics market growth has created new opportunities and additional demand for some service robotics applications. Such as professional cleaning, logistics robots. Medical robotics is the robotics segment with the highest growth rate. [2].

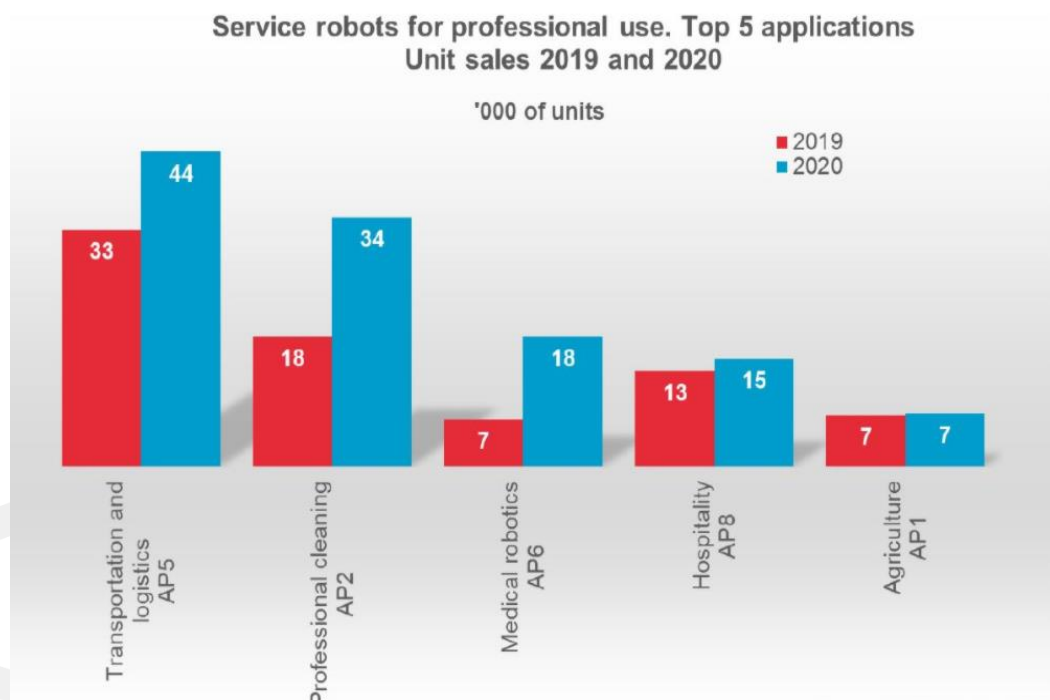


**Figure 2** TOP 5 applications for professional use [5]

As aforementioned, the development of new types of robots in order to support the new services are highly required with reasonable cost, high performances. We are therefore interested to do research in these areas.

## **Charging modes for mobile robots**

The charging mode of a mobile robot depends on the operating performance of the battery and the charging requirements. There are different standards for battery charging, with a wide variety and different performance, which makes the charging modes very different. Currently, there are three main charging modes such as regular charging, fast charging, and battery replacement [6].

### **1. Conventional charging mode**

When the battery is discharged to a low voltage state, the charging current is generally small, with a current of about a dozen amps, and this charging mode is generally referred to as the conventional charging mode. Conventional charging is also called AC slow charging, grid AC power is converted to DC power by the charger, and the battery is charged with a low current constant current or constant voltage charging, and the charging time is generally 5 to 8 hours. The advantages of the traditional charging method are that the design and installation cost of the charger is relatively low, and the charging process of the mobile robot can be carried out during low power hours, which can effectively reduce the charging cost, improve the charging efficiency and extend the service life of the battery. The disadvantage of the traditional charging method is that the charging time is long and it is difficult to meet the charging demand during the peak power consumption period.

### **2. Fast charging mode**

As the traditional charging method of mobile robot battery has a high time cost and does not match the working hours of the mobile robot, the fast charging method has emerged. Fast charging, also called DC fast charging, charges the battery directly through a DC charging device, and the charging current can generally reach hundreds of amperes, providing a shorter charging time for the battery by means of high-current charging. The advantage of the fast charging method is that the charging time is short, which can extend the battery life. However, it is less efficient and more costly than traditional charging methods. In addition, its safety requirements are relatively more stringent due to the high current generated during fast charging.

### **3. Battery replacement method**

The battery replacement method, also known as the mechanical charging method, recharges the mobile robot by directly replacing the battery when the mobile robot battery runs out of power. This method is not only convenient and fast but also can improve the efficiency of the mobile robot. In addition, it is also possible to charge the replaced battery at night, which results in lower electricity costs and increased flexibility in the use of the mobile robot. However, since the batteries of mobile robots are heavy, the battery replacement process is correspondingly difficult.

In terms of charging time and work efficiency, the battery replacement method and the fast charging method have relatively shorter charging times and are more in line with the needs of users. However, in terms of charging cost, charging safety, and charging efficiency, the advantages of the traditional charging method are more

obvious, so the traditional charging method is still an irreplaceable charging method for mobile robots.

### **Project Importance**

One of the most important parts of the robots is the power supply that helps to convert supplying power into the most suitable amount and levels. A high power rating power supply would provide more robust and retain greater power conversion compared to a low power rating power supply. But would encounter some problems related to the investment costs, power losses, larger size, and heavier weight. As a result, this causes the crucial demand for optimum mobility and miniaturization that has led to the development of miniaturization of the various modules of the robots. In addition, the volume of the power module is also a major factor that restricts the volume and portability of the robots. Due to the fact that the volume and heat dissipation limitations of the power device. Therefore, designing a power supply with high efficiency, small size, and low heat generation is particularly important for the development of the robotics industry.

In this recent years, the GaN based electronic devices would possibly be used to replace the conventional Si based electronic devices used nowadays due to their higher power density rating, smaller size, and lighter weight. There are some research works that have been studied on these devices available in literatures[7-14]. But performance in terms of efficiency and performance compared to the Si based devices has not been properly compared. In this research, the comparison of GaN based switching devices for the most suitable totem-pole bridgeless for AC power conversion and the half-bridge LLC circuit for DC power conversion used in commercial robot power supply adaptors in terms of efficiency, power quality, and dynamic response performances will be examined and compared to the conventional Si based switching devices. The results from both simulation and experimental tests will be used to validate the research study.

### **Purposes of Research**

The purpose of this research is to study, design, and construct a power supply with GaN based switching devices compared to the conventional Si based switching devices, which could satisfy the following features:

1. Suitable size and weight for the service robot equipment (such as Automated Guided Vehicle (AGV), Autonomous Mobile Robot (AMR), Drones, etc.)
2. Higher efficiency
3. Better power quality and dynamic responses



## CHAPTER II

### LITERATURE REVIEW

To power robots to perform actions as commanded, the suitable levels and amount of electric power have to be managed before supplying the robots. Commonly, there are 2 main parts concerned which are the power conversion part and the battery charger part. The power conversion part of a typical power supply consists of several electronic devices or circuits. The battery charger consists of an EMI filter, an AC-DC power factor correction (PFC) converter to charge from the grid, and a DC-DC converter to regulate the voltage across the storage. In this research, the power conversion part will be considered.

There are 2 main components of the power conversion part under this study: AC power conversion and DC power conversion, respectively:

#### AC-DC

AC power from the grid is used to provide power to the service robot. Therefore, the AC power from these sources must be converted to a suitably sized DC power before it can be fed to the robot. There are many types of AC power conversion circuits available, and the rectifier bridge of a conventional rectifier filter circuit is only turned on when the input sine wave voltage is near its peak. As a result, the input electrical process generates severe non-sinusoidal waves, leading to a large harmonic current component in the input, reducing the utilization of the grid and potentially interfering with other appliances[15-19]. However, in this study, the most commonly used power factor correction (PFC) will be considered, where the pre-stage PFC circuit has two functions, one is to stabilize the DC bus voltage to provide a larger input voltage for the post-stage circuit, and the other is to improve the system power factor to avoid harmonic pollution to the grid. There are various methods to improve the power factor, among which the active power factor correction method is widely used because of its simple structure, convenient control, and the best correction effect[20]. The active power factor correction method reduces the current harmonic pollution by controlling the grid current waveform as a sinusoidal waveform with the same frequency and phase as the grid voltage to improve the system power factor, and the common topologies are Buck circuit, Boost circuit, Cuk circuit and Zeta circuit[21]. Cuk and Zeta circuits are relatively complex, using two inductors, although their input and output currents are smoother, their size and mass are larger. This paper will use the Boost PFC circuit as an AC-DC circuit.

There are currently six bridgeless PFC topologies, as shown in Figure 3.

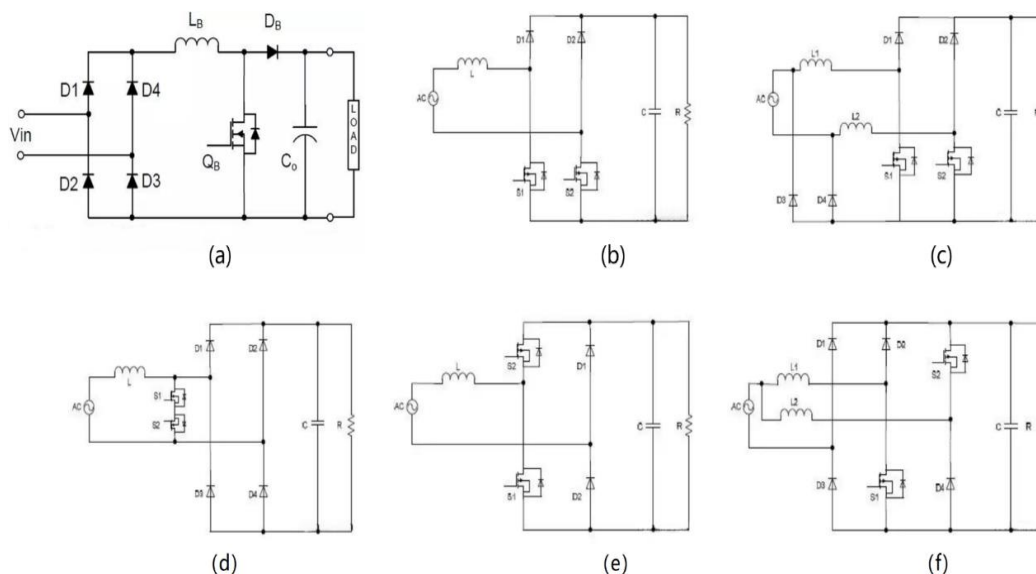


**Figure 3** PFC converters (a) Diode bridge converter [22], (b) Symmetrical bridgeless [23], (c) Symmetrical bridgeless with common mode filter [24], (d) Two-way switch bridgeless PFC [15], (e) totem-pole bridgeless [25], (f) Fake Totem Pole PFC

The detailed features of these 6 PFC topologies are as follows:

(a) Diode bridge converter [22]

The diode bridge converter has 2 diodes (rectifier bridges) turned on each time, and a MOS or boost diode is turned on, that is, 3 power devices are turned on each time, and the loss is large.

(b) Symmetrical bridgeless [23]

When this kind of PFC is in the positive and negative half cycle, two semiconductor components, one freewheeling, and the other acting as a high-frequency switch.

The advantage of this topology is that fewer power components are used, and the two transistors can be driven together, which simplifies the design of the drive circuit and makes it possible to directly use the traditional APFC control chip.

However, it has several problems at the same time. The current flow is complicated and does not share the ground, current sampling is difficult, and there is a large common-mode interference. Therefore, the input filter must be carefully designed.

(c) Symmetrical bridgeless with a common mode filter

This topology is improved from Symmetrical bridgeless, adding D3 and D4 as low-frequency current loops, and S1 and S2 only serve as high-frequency switches without participating in low-frequency freewheeling. Same as the standard bridgeless PFC, S1, and S2 can be driven at the same time, and inserting a sampling resistor after the two low-frequency diodes D3 and D4 can simply sense the current like a normal

PFC. At the same time, this topology has a lower common-mode current. However, this topology must use two inductors, the current flow is uncertain, the low-frequency diode and the body diode of the MOS may be turned on at the same time, which increases the instability factor.

(d) Two-way switch bridgeless PFC [15]

S1 and S2 form a two-way switch, they can be driven at the same time, the current can be easily detected by using a current transformer, D1 and D3 are ultra-fast recovery diodes, and D2 and D4 can use low-frequency diodes. The disadvantage is that the potential of the entire circuit changes drastically with respect to the ground, which will cause a more serious EMC problem than Symmetrical bridgeless. The output voltage cannot be directly sampled, and isolation sampling is required.

(e) Totem-pole bridgeless [25]

Evolved from Symmetrical bridgeless, but the principle is slightly changed. D1 and D2 are low-frequency diodes, and the body diodes of S1 and S2 provide high-frequency rectification switching functions. This kind of circuit has lower EMI, uses fewer components, and the design can be very compact. But S1 and S2 need to use different driving signals, and the signals are different for different power frequency cycles, which increases the complexity of control, and S2 is not easy to drive. If S1 and S2 use MOSFET, the body diode of MOSFET has a slower recovery (usually hundreds of ns), which will generate a larger current backflow pulse, causing a large loss, which is enough to offset the advantage of bridgeless and low loss. If S1 and S2 use IGBTs, although the performance of their body diodes is no problem, their turn-on voltage drops are relatively large, and high losses will also be generated, especially in the case of low voltage input.

(f) Fake Totem-Pole PFC

Evolved on the basis of totem-pole bridgeless, D2 and D4 replace the freewheeling effect of the original body diodes inside S1 and S2. The control method is the same as totem-pole bridgeless. This topology requires two inductors, the utilization rate is not high, the volume is large, and S2 is extremely difficult to drive.

Among the above 6 PFC topologies, (a) has excessive losses, (b) and (d) have more serious EMI problems, and (c) and (f) have fewer EMI problems, but additional components are required. Totem-pole bridgeless PFC(e), which belongs to the bridgeless PFC family, can not only save conduction loss, especially at low line voltages but also emits less common mode EMI noise [15, 26, 27]. Therefore, the Totem-pole bridgeless PFC topology is the best choice for the AC-AD link in this study.

## DC-DC

DC-DC circuits generally require it to be small to reduce the size and mass of the power supply. One of the main means of miniaturization is to reduce the size of the energy storage components in the circuit by increasing the switching frequency of the switching transistors. However, as the switching frequency increases, the switching

losses of the switching transistors also increase, which can lead to serious system heat generation and increase the difficulty of heat sink design. Therefore, DC-DC circuits generally use soft-switching technology to achieve zero-voltage switching or zero-current switching of the switching transistors to reduce the switching losses. Common DC-DC converters include zero-switching PWM converters, zero-conversion PWM converters, phase-shifting full-bridge converters, quasi-resonant converters, and fully resonant converters [28, 29].

Zero-switching PWM converters and zero-conversion PWM converters realize the soft switching process of the main switching transistors by adding auxiliary circuits and switching transistors, which only shift the losses and do not reduce them, and increase the complexity and cost of the circuit. Phase-shifted full-bridge converters operate by shifting the switching transistors to complement each other's conduction and resonate with the converter to realize the soft-switching process of the switching transistors without adding additional circuitry, but the primary current is larger, the conduction loss is larger, and the duty cycle is lost. The quasi-resonant converter can only make the circuit work in the resonant state in a specific period of time, but not at other times, when the switching process is hard switching, which will produce large switching losses.

Unlike traditional PWM (Pulse width modulation) converters, LLC is a resonant circuit that achieves a constant output voltage by controlling the switching frequency (frequency adjustment).

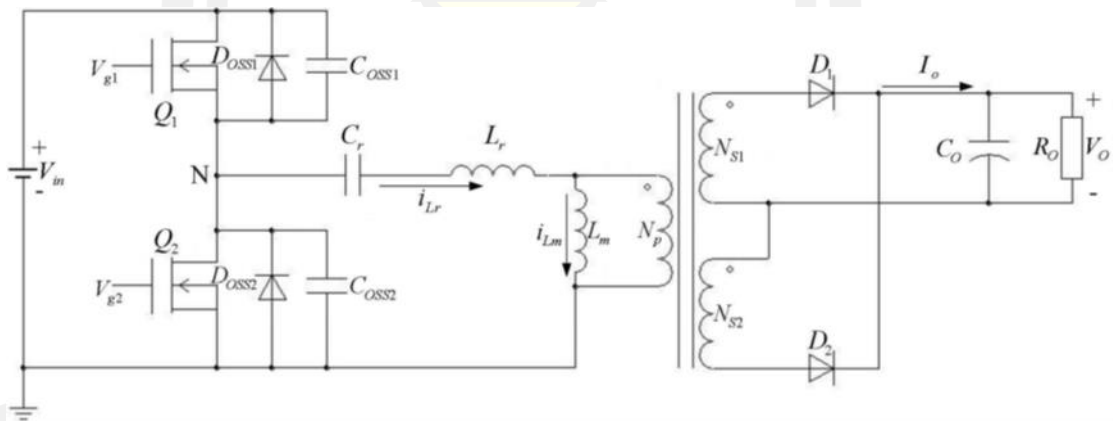


**Figure 4** LLC converter topology [25]

To manage the voltage across the battery, the half-bridge LLC resonant converter [30-36] is used as a DC-DC converter. This converter is particularly common because it switches at zero voltage across a large input voltage range, resulting in reduced switching losses. As a result, LLC converters may be utilized to alter the PFC converter output (380-400V) to double the fundamental frequency ripple to 48V for battery charging applications. Another feature of this converter is its ability to transition softly over the whole load range [37]. The switching loss of the power supply can be decreased using soft switching technology, and the efficiency and power density of the power converter may be enhanced.

## Control Strategy

### 1. Boost PFC circuit control strategy

Boost PFC circuits have two control objectives: one is to make the output voltage stable, and the other is to make the power factor close to 1. Boost PFC circuits have three control strategies: continuous current mode (CCM), intermittent current mode (DCM), and critical current mode (BCM) [38].

The inductor current under CCM control is continuous, with small ripple and low THD, which is beneficial to the design of the filter inductor, while the output voltage fluctuation is small and the output capacitor requirement is not high, but the CCM control structure is complex and requires measuring both the grid voltage and inductor current. BCM control is between CCM control and DCM control, but it generates a large current loop, which makes the switch tube undergo large current stress. In order to meet the requirements of the high power factor of the power supply, the CCM control method with better overall performance should be selected.

### 2. LLC resonant converter control strategy

There are four basic control strategies for LLC circuits: pulse frequency modulation (PFM) [39-41], phase shift modulation (PSM), pulse width modulation (PWM), resonant frequency modulation (RFM) [42].

The traditional control strategy for LLC converter is pulse frequency modulation (PFM). The resonant tank impedance distribution is modified by adjusting the switching frequency and ultimately regulates the output voltage.

Phase shift modulation (PSM) can regulate the converter at a constant switching frequency. The phase shift can be applied either on the primary side or the secondary side. For primary side PSM (PSPSM) [43, 44], the converter is regulated by modifying the inverter output voltage waveform. The soft switching operation for the lagging leg is very challenging, which cannot be satisfied with a large phase shift angle. Thus, the suitable operating voltage gain range is restricted. On the other hand, the secondary side PSM (SSPSM) [45] can be utilized to regulate the LLC converter, the secondary unregulated rectifier diodes are replaced with MOSFETs to implement phase shift control on the secondary side. Therefore, the output voltage regulation is achieved with SSPSM.

Pulse width modulation (PWM) as a common control strategy can also be applied for LLC converter. If the PWM control is applied on the primary side, it is called PSPWM [46]. Thus, the output voltage can be regulated based on the percentage of either full-bridge operation or half-bridge operation. Generally, the issues with these control strategies are high cost and low power density due to the additional components.

Resonant frequency modulation (RFM), which can dynamically adjust the resonant tank components' impedance. Thus, the voltage gain is adjusted. For RFM, the essence of the output voltage regulation is the control of the normalized switching frequency. If the switching frequency is kept constant, then, by adjusting the resonant

frequency, the normalized switching frequency can also be modified, and finally, the output voltage is regulated.

Considering the power supply requirements for efficiency, pulse frequency modulation (PFM) control is more suitable for fully resonant converters.

### Power supply complete topology

Based on the above comparative selection of AC-DC converter and DC-DC converter respectively, the overall topology of the power supply can be obtained as shown in Figure 5. Among them, the PFC circuit adopts the totem-pole bridgeless PFC circuit to reduce the system loss and improve the system efficiency by using its feature of fewer components and no rectifier bridge; the DC-DC converter adopts the full-bridge LLC resonant converter to reduce the switching tube loss by using its feature of soft switching of power tubes, thus further improving the system efficiency.

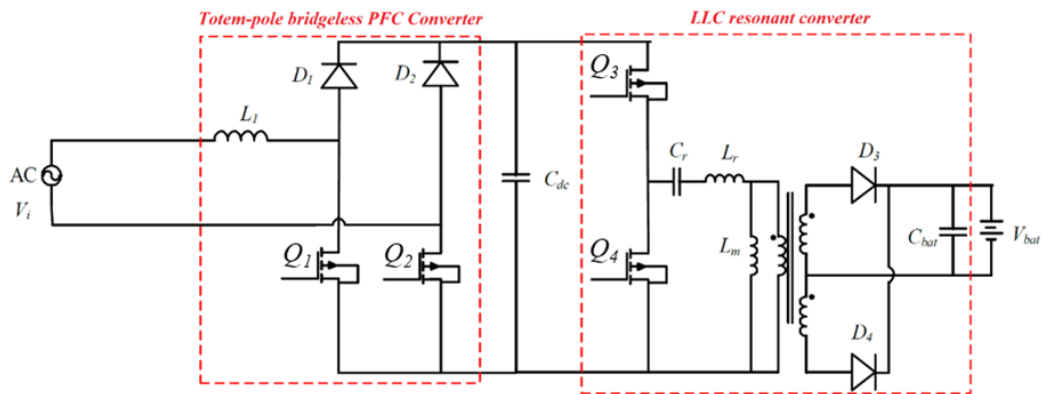


**Figure 5** The converter configuration of the proposed system.

### Selection of semiconductor devices

The largest portion of the power losses in power electronic converters is dissipated in their power semiconductor devices. Currently, these power devices are based on the mature and very well-established Si technology although Si exhibits some important limitations regarding blocking voltage capability, operation temperature, and switching frequency. At present, the highest commercial Si IGBT breakdown voltage capability is 6.5 kV with limited switching performance, and not any Si-based device may operate above 200 °C. These unavoidable physical limits reduce drastically the efficiency of current power converters, which require among others, complex and expensive cooling systems and expensive passive components. Consequently, a new generation of power devices based on wide bandgap (WBG) semiconductor materials is expected for power converters. The use of these new WBG power semiconductor devices will allow increasing the efficiency of the electric energy transformations achieving a more rational use of the electric energy together with a considerable improvement in size and robustness of power converters.

Among the possible semiconductor materials candidates, Silicon Carbide (SiC) and Gallium Nitride (GaN) show the best tradeoff between theoretical characteristics (high blocking voltage capability, high-temperature operation, and high switching

frequencies), real commercial availability of the starting material (wafers and epitaxial layers), and maturity of their technological processes. Figure 6 highlights some key material properties of WBG semiconductor candidates to replace Si [47, 48].

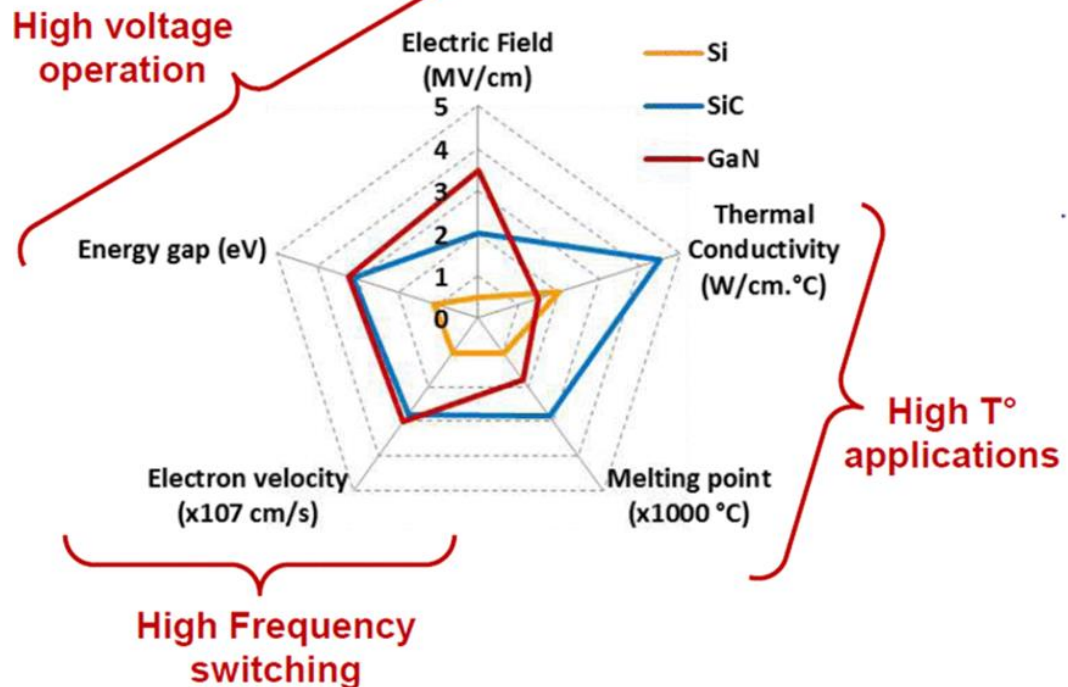
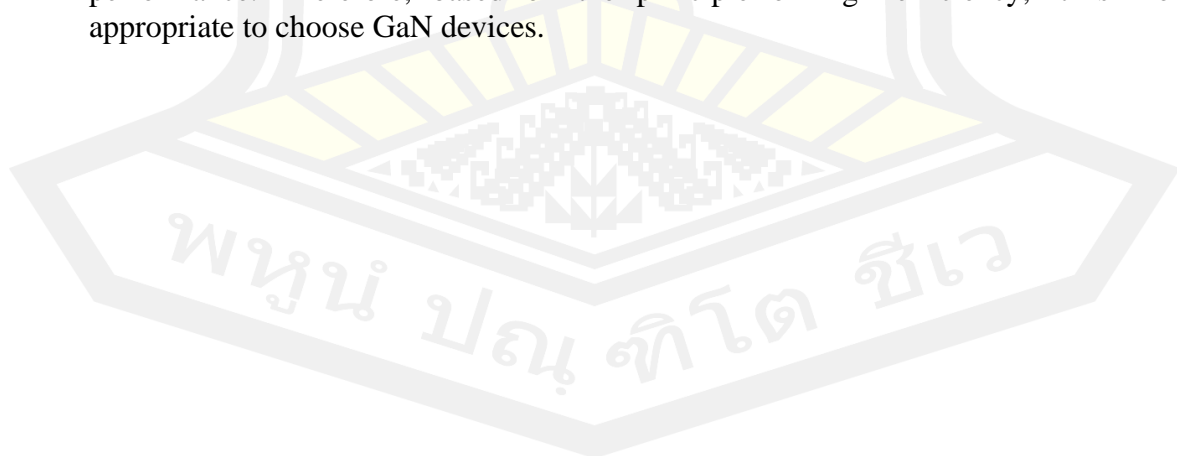


**Figure 6** Summary of Si, SiC, and GaN relevant material properties [49]

The breakdown voltage of SiC and GaN is 10 times higher than that of Si, which makes them suitable for high voltage applications. SiC has higher thermal conductivity than both GaN and Si, which makes it more suitable for high temperature and high power applications. In terms of comprehensive parameters, GaN has the best performance. Therefore, based on the principle of high efficiency, it is more appropriate to choose GaN devices.



## CHAPTER III

### METHODOLOGY

#### Totem-pole bridgeless PFC control logic

Figure.7 shows simplified equivalent operation principles of the Totem-pole bridgeless PFC circuit. There are 4 modes of operation as explained belows:

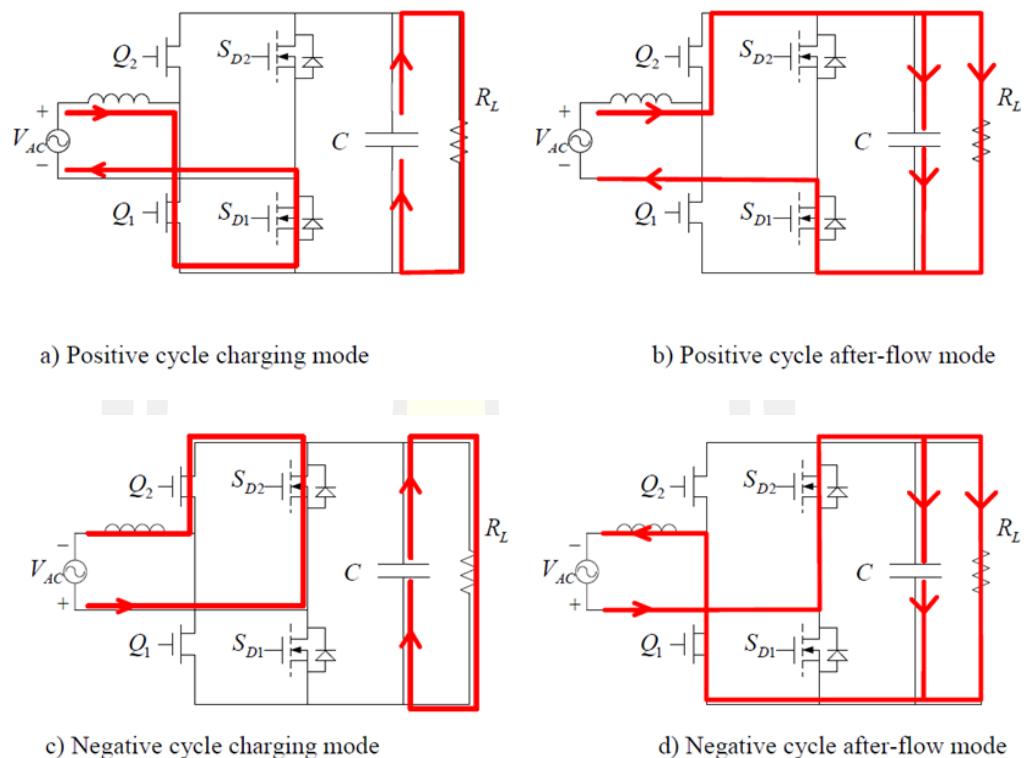


**Figure 7** Totem-pole bridgeless PFC simplified illustration [17]

The GaN transistors Q1 and Q2 form a high-frequency bridge arm operating in the high-frequency PWM mode, and the Si MOSFET transistors S1 and S2 with low on-resistance form a low-frequency bridge arm operating in the industrial frequency switching cycle, in the positive half-cycle of the input voltage, the Si MOSFET transistor S1 turns on while the Si MOSFET transistor S2 turns off, and in the negative half-cycle of the input voltage, the Si MOSFET transistor S2 turns on while Si MOSFET transistor S1 turns off.

When the input voltage is positive half-cycle, the circuit is divided into two operating modes: when Q1 is on, the input current charges the inductor L through the high-frequency switching transistor Q1 and Si MOSFET transistor S1, and the energy required by the load is provided by the capacitor C. When the high-frequency switching transistor Q1 is off, the high-frequency switching transistor Q2 is on, and the current path at this time is the power supply L terminal — inductor L — high frequency switching transistor Q2 — load — Si MOSFET transistor S1 — power supply N terminal, the input power, and inductor together to supply the load. When



the input voltage is negative half-cycle the circuit is divided into two operating modes: when the high-frequency open-switching transistor Q2 is on, the input current

through the high-frequency on-switching transistor Q2 and Si MOSFET transistor S2 to charge the inductor L. The energy required by the load is provided by the capacitor C, when the high-frequency on-switching transistor Q2 is off, the high-frequency on-switching transistor Q1 is on, and the input power and the inductor L jointly supply the load through the Si MOSFET transistor S2 and the high-frequency on-switching transistor Q1.

From the above modal analysis, it is clear that the primary side current path contains only one high-frequency switching transistor and one low-frequency switching transistor, and there is no diode voltage drop. In the positive AC voltage cycle, two GaN high electron mobility transistors Q1 and Q2 form the Boost synchronous rectifier circuit, while one transistor Q1 acts as the master switch to make the power supply charge the inductor, the other transistor Q2 acts as the slave switch to make the power supply and the inductor jointly supply the load, while in the negative AC voltage cycle, the master and slave functions of two GaN high electron mobility transistors Q1 and Q2 are switched.

In order to prevent the bridge arm from going through, a dead time must be set between the two GaN high electron mobility transistors Q1 and Q2. It is possible to operate in continuous conduction mode.

### Design of the Totem-pole bridgeless PFC Converter Parameters

SYMBOL	PARAMETER	MINIMUM	NOMINAL	MAXIMUM	UNIT
$V_{in}$	AC input voltage	100	230	264	V AC
$f_{line}$	Line frequency	47	50	63	Hz
$V_{out}$	Output voltage		385		V DC
$P_{out(nom)}$	Output power			550	Watt
$\eta$	Targeted efficiency		99%		
iTHD	Targeted input current THD		<5% @>30% Load		
PF	Targeted power factor		0.98		
$F_{sw}$	Switching frequency		500 k		Hz

**Table 1** Target design parameters for the PFC stage

First, determine the maximum average output current,  $I_{OUT(max)}$  as Equation 1:

$$I_{out(max)} = \frac{P_{out(max)}}{V_{dc\_link}} = \frac{550W}{385V} = 1.43A \quad (1)$$

The maximum input RMS line current,  $I_{IN\_RMS(max)}$ , is calculated using the parameters from Table.1, and the efficiency and power factor initial assumptions are calculated as follows:

$$I_{INrms(max)} = \frac{P_{OUT(max)}}{\eta_{PFC} \times V_{IN(min)} \times PF} = \frac{550W}{99\% \times 100V \times 0.98} = 5.67A \quad (2)$$

To determine the boost inductor, the maximum-allowed ripple current is calculated first. The maximum ripple current is observed at the lowest input voltage and maximum load. Assuming a maximum 40% ripple in the inductor current, the ripple current would be calculated as follows:

$$I_{INripple(max)} = \frac{V_{OUT(max)} - \sqrt{2}V_{IN(min)}}{V_{dc.link}} = \frac{385V - \sqrt{2} \times 100}{385} = 0.63 \quad (3)$$

The minimum value of the boost inductor is calculated based on the acceptable ripple current, at a worst-case duty cycle of 0.63:

$$L_{Boost} \geq V_{OUT(max)} \times DUTY_{(max)} \times \frac{1 - DUTY_{max}}{F_{sw} \times I_{INripple(max)}} = 160\mu H \quad (4)$$

The output capacitor,  $C_{bus}$ , is sized to meet the DC link ripple and holdup requirements of the converter. The ripple of DC link voltage can be calculated by Equation 5:

$$V_{ripple} = \frac{P_{OUT} \times 0.0032}{C_{bus} \times V_{bus}} \quad (5)$$

The holdup time required by this design,  $T_{Holdup}$  is 2ms. The average bus voltage is set at 385V, which is correlated with the LLC transformer ratio. Considering the DC link voltage has a +/-10V ripple at full load, the DC BUS voltage will be  $V_{BUS(norm)} = 365V$  in the valley point.

Considering the gain of LLC can not be too wide, the minimum input of LLC is set at  $V_{BUS(min)} = 320V$ . For energy, the minimum value of BUS capacitance can be calculated using Equation 6.

$$\begin{aligned} C_{OUT} &\geq 2 \times P_{OUT(nominal)} \times \frac{T_{Holdup}}{V_{OUT(norm)}^2 - V_{OUT(min)}^2} \\ &= 2 \times 500 \times \frac{2ms}{365^2V - 320^2V} = 130\mu F \end{aligned} \quad (6)$$

Considering that in the subsequent analysis, GaN and Si MOS need to be used for simulation comparison analysis, all parameters need to be consistent, so the input and output indicators of the power supply and related main power device parameters are as follows:

Input current ripple inductor:  $L_{boost} = 1000 \mu H$

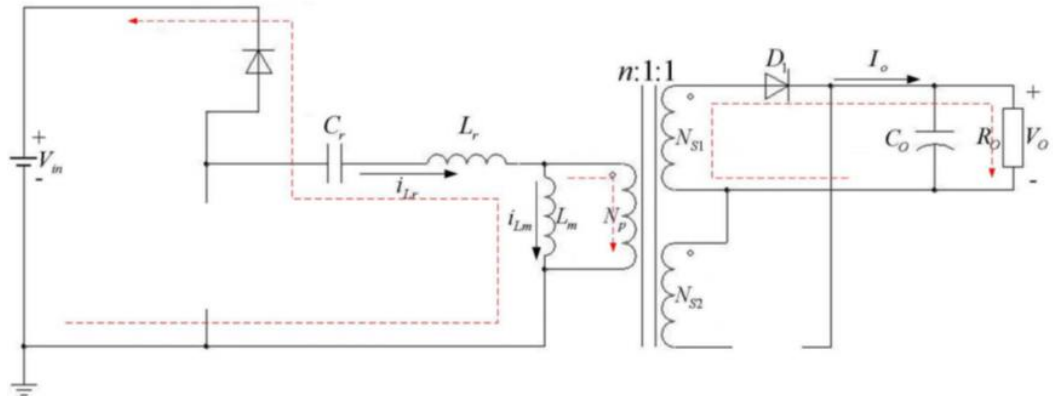
Output filter capacitor:  $C_{out} = 660 \mu F$

Power frequency Si MOS transistors selection: ipw65r041cfd

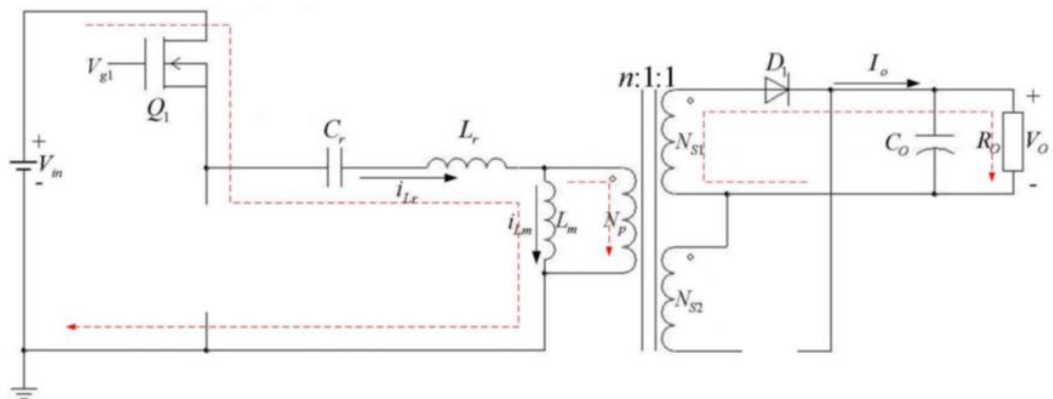
## LLC resonant converter control logic

### 1. How it works when $f_m < f < f_s$

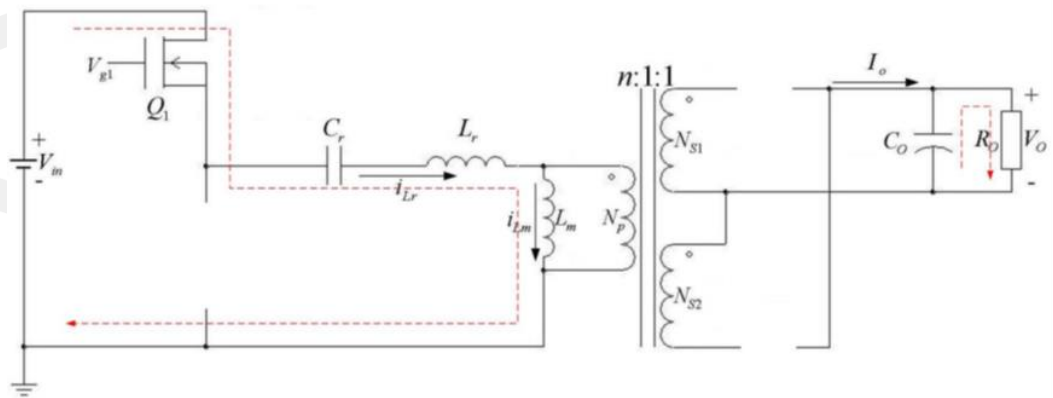
When the operating frequency is  $f_m < f < f_s$ , The equivalent circuit of each operating phase is shown in Figure 8. The operating waveform of the LLC resonant converter is shown in Figure 9. According to Figure 9, one switching cycle can be divided into 8 operating phases.



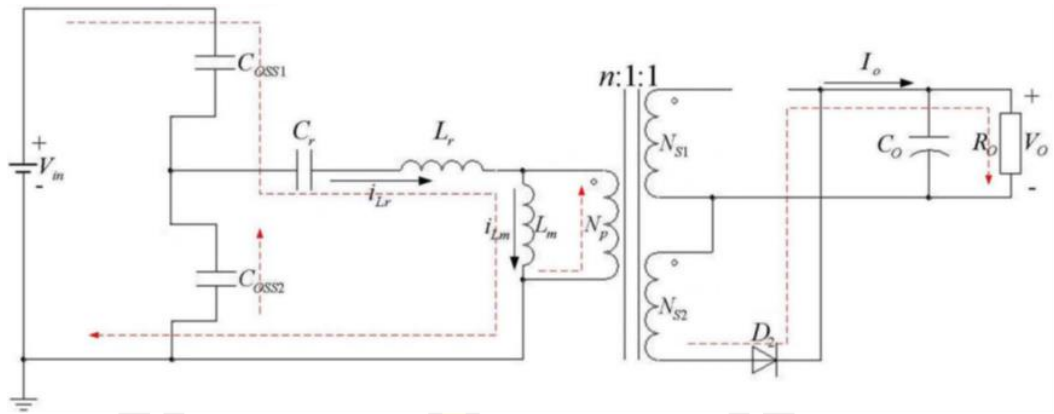
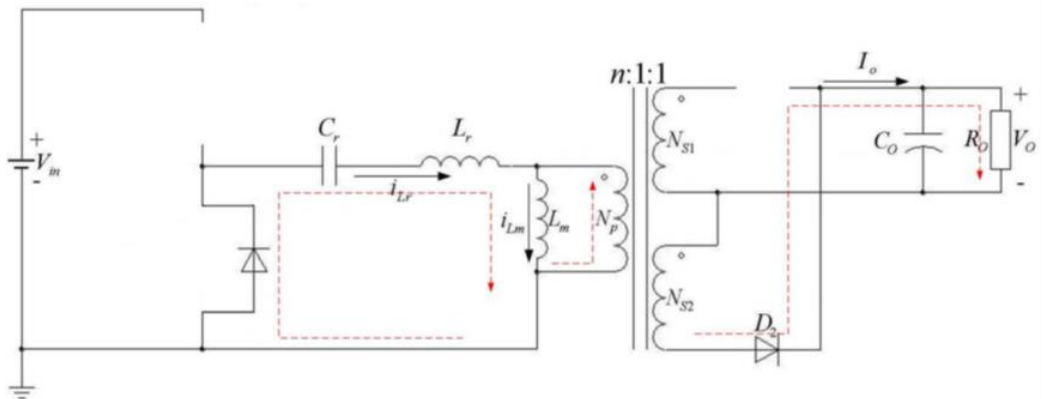
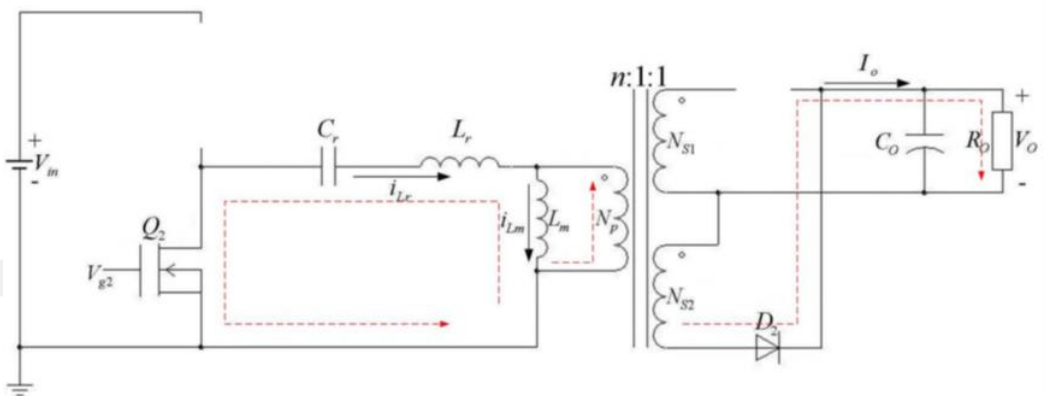
Phase1 (  $t_0 < t < t_1$  )

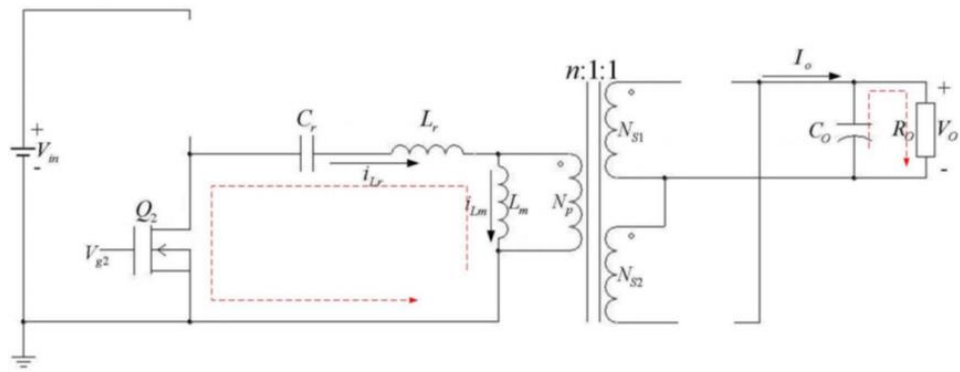


Phase2 (  $t_1 < t < t_2$  )

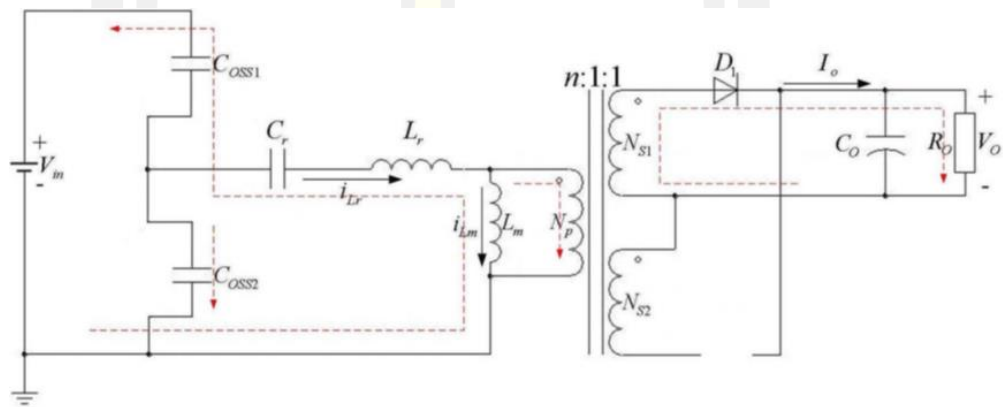


Phase3 (  $t_2 < t < t_3$  )

Phase4 (  $t_3 < t < t_4$  )Phase5 (  $t_4 < t < t_5$  )Phase6 (  $t_5 < t < t_6$  )



Phase7 ( $t_6 < t < t_7$ )



Phase8 ( $t_7 < t < t_8$ )

**Figure 8** LLC resonant circuit Operation sequence with  $f_m < f < f_s$

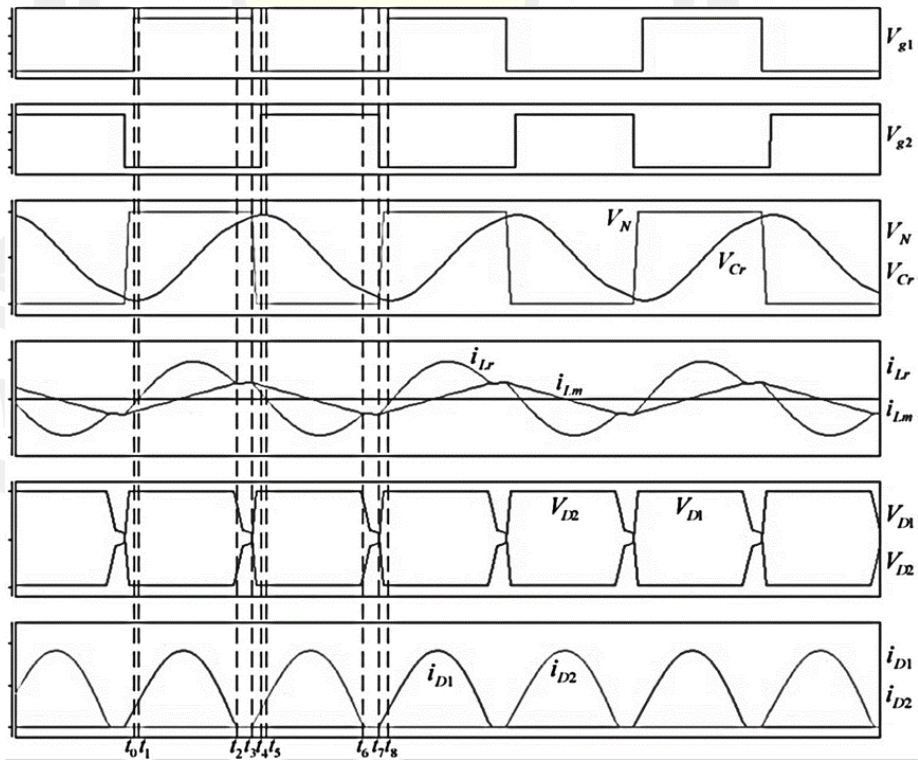


**Figure 9** LLC resonant circuit Operation waveforms with  $f_m < f < f_s$

#### Phase 1 ( $t_0 < t < t_1$ )

At the moment  $t_0$ , Q2 turns off and the circuit enters the phase 1 state, when the current flowing through the resonant inductor  $L_r$  is negative, so the body diode of Q1 conducts, creating the conditions for the ZVS of Q1 to conduct. The energy in this stage is fed back to the input  $V_{in}$ .

When the body diode of Q1 conducts,  $i_{Lr}$  starts to increase and the polarity of the primary side of the transformer is up positive and down negative, forcing the secondary diode D1 to conduct and the transformer starts to output voltage at the secondary.  $nV_o$  on  $L_m$  is clamped by the output voltage so that only  $L_r$  and  $C_r$  are involved in resonance and  $L_m$  is charged at constant voltage during this process.

At the moment  $t_1$ , the resonant current  $i_{Lr}$  rises to 0 and the phase 1 operating state ends.

#### Phase 2 ( $t_1 < t < t_2$ )

When the resonant inductor current  $i_{Lr}$  changes from negative to positive, it enters the working phase 2. Q1 has been added to the gate turn-on signal in phase 1, so it turns on positively at the moment of  $t_1$ , at which time the rectifier diode D1 turns on and the transformer primary voltage is clamped at  $nV_o$ ,  $L_m$  is charged linearly at this voltage and does not participate in resonance. At this phase, the whole circuit resembles a series of resonant circuit with resonant inductor  $L_r$  and resonant capacitor  $C_r$ , and energy is transferred from input  $V_{in}$  to  $V_o$ .

At the moment  $t_2$ , the  $L_r$  current is equal to the  $L_m$  current and the phase 2 operating state ends, when the current of the output diode D1 becomes 0.

#### Phase 3 ( $t_2 < t < t_3$ )

At time  $t_2$ , the current  $i_{Lr}$  of inductor  $L_r$  is equal to the current  $i_{Lm}$  of inductor  $L_m$ , rectifier diodes D1 and D2 are reverse biased and cut off, the output is isolated by the transformer, and  $L_m$  starts to participate in resonance, forming a resonant circuit in series with  $L_r$  and  $C_r$ . The output capacitor  $C_o$  discharges and continues to supply power to the output.

Q1 turns off at  $t_3$  and the phase 3 operating state ends.

#### Phase 4 ( $t_3 < t < t_4$ )

At  $t_3$ , Q1 and Q2 turn off and enter the dead time. The resonant current charges the parasitic capacitor  $C_{oss1}$  of Q1 and discharges the parasitic capacitor  $C_{oss2}$  of Q2. At this time, the current in  $L_m$  is larger than the current in  $L_r$ , and the difference between them flows through the primary side of the transformer, and the rectifier diode D2 starts to conduct.

At  $t_4$ , the discharge of  $C_{oss2}$  ends, and the body diode of Q2 turns on, at which point the phase 4 operating state ends.

#### Phase 5 ( $t_4 < t < t_5$ )

At  $t_4$ , Q1 is still off and the body diode of Q2 is on, creating the conditions for the ZVS of Q2 to be on.

At this time, the rectifier diode D2 is on and the transformer primary voltage is clamped at  $-nV_o$ , which is negative and positive.  $L_m$  is linearly charged at this voltage and does not participate in resonance, only  $L_r$  and  $C_r$  participate in resonance, and the resonant current flows through  $L_m$  and the primary side of the transformer and the body diode of Q2, and the energy is transferred to the output  $V_o$ .

At the moment  $t_5$ , the resonant current  $i_{Lr}$  drops to 0 and the phase 5 operating state ends.

Phase 6 (  $t_5 < t < t_6$  )

At  $t_5$ , Q1 is turned off and Q2 is on. At this time, the rectifier diode D2 is on, and the transformer primary voltage is clamped at  $-nV_o$ , with negative upper and positive lower.  $L_m$  is linearly charged at this voltage and does not participate in the resonance. Only  $L_r$  and  $C_r$  participate in the resonance, and the resonant current flows through  $L_m$  and the primary side of the transformer, transferring energy to the output  $V_o$ .

At  $t_6$ , the  $L_r$  current is the same as the  $L_m$  current and the phase 6 operating state ends, when the current of the output diode D2 becomes 0.

Phase 7 (  $t_6 < t < t_7$  )

At  $t_6$ , the current of inductor  $L_r$  and inductor  $L_m$  are equal, rectifier diodes D1 and D2 are reverse biased and cut off, the output is isolated by the transformer, and  $L_m$  starts to participate in resonance. The resonant current circulates in Q2 and the resonant cavity. The output capacitor  $C_o$  discharges and continues to supply power to the output  $V_o$ .

The phase 7 operating state ends when Q2 is turned off at  $t_7$ .

Phase 8 (  $t_7 < t < t_8$  )

At  $t_7$ , Q1 and Q2 turn off and enter the dead time. The resonant current charges the parasitic capacitor  $C_{oss2}$  of Q2, and discharges the parasitic capacitor  $C_{oss1}$  of Q1. Since the current in  $L_r$  is larger than the current in  $L_m$ , the difference between the two flows through the primary side of the transformer, and the rectifier diode D1 starts to conduct.

At  $t_8$ , Q1 starts to conduct and the circuit enters the next cycle.

## 2. How it works when $f = f_s$

Figure 10 shows the operating waveform of the LLC resonant converter at  $f = f_s$ . When  $f = f_s$ , this operating state is a special case of  $f_m < f < f_s$ . In contrast to operation at  $f_m < f < f_s$ , there are only six operating phases, without phase 3 and phase 7. At this time, the resonant current is a pure sine wave, and the currents in rectifier diodes D1 and D2 are critically continuous.

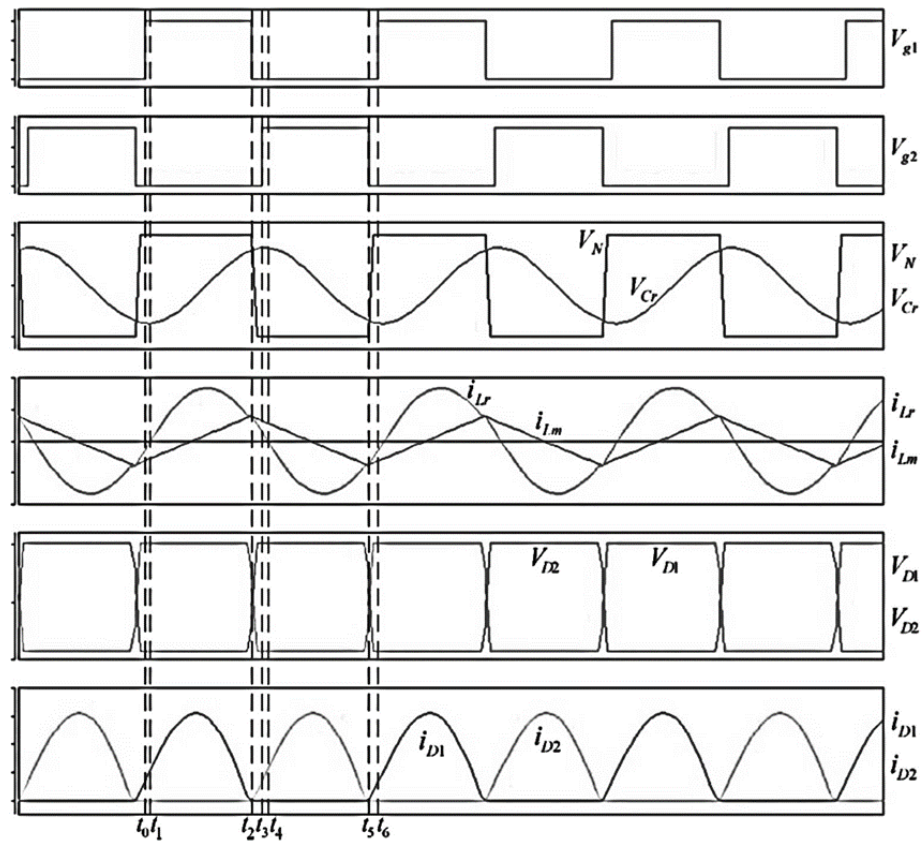
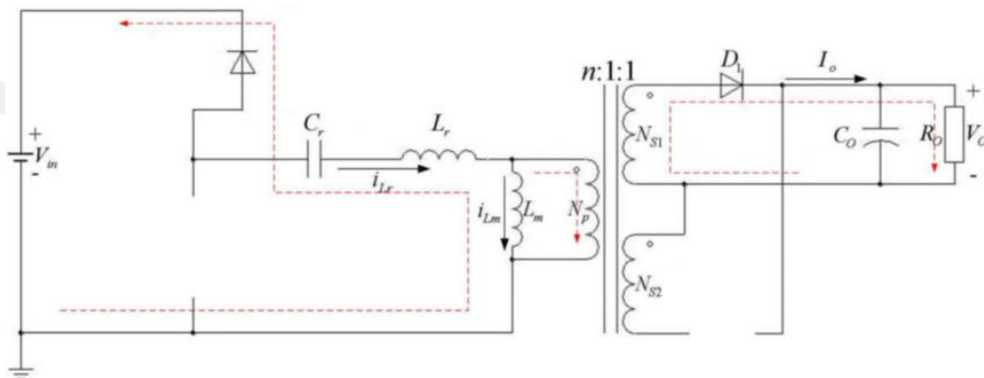


**Figure 10** LLC resonant circuit Operation waveforms with  $f = f_s$

### 3. How it works when $f > f_s$

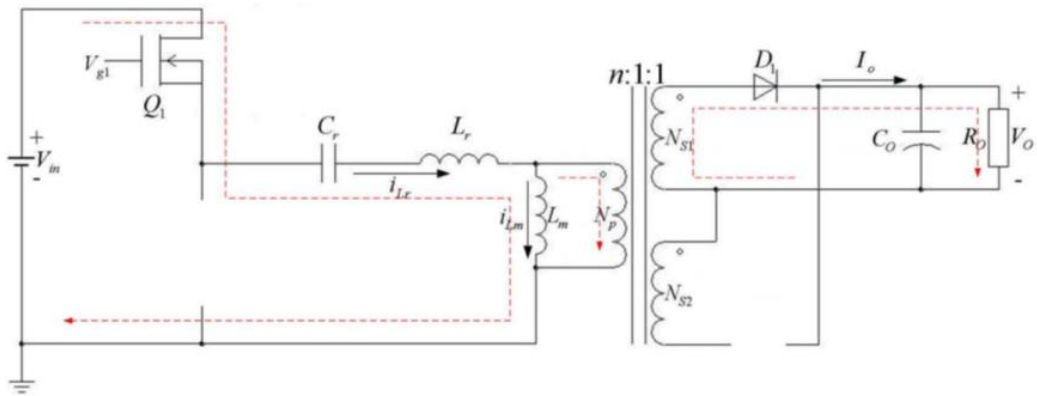
When the LLC resonant converter operates at  $f > f_s$ , the equivalent circuit of each operating phase is shown in Figure 11, and the main operating waveforms are shown in Figure 12. According to Figure 12, one switching cycle can be divided into 8 operating phases.

The operating characteristics of the LLC resonant converter are similar to those of the series resonant converter when  $f > f_s$ .  $L_m$  never participates in the resonance and is always clamped by the output voltage.  $L_m$  is never involved in resonance and is always clamped by the output voltage.

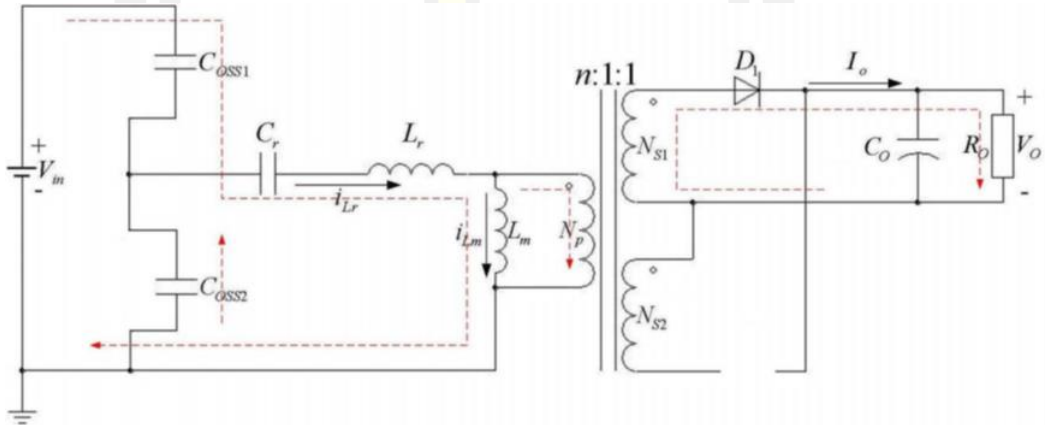


Phase1 (  $t_0 < t < t_1$  )

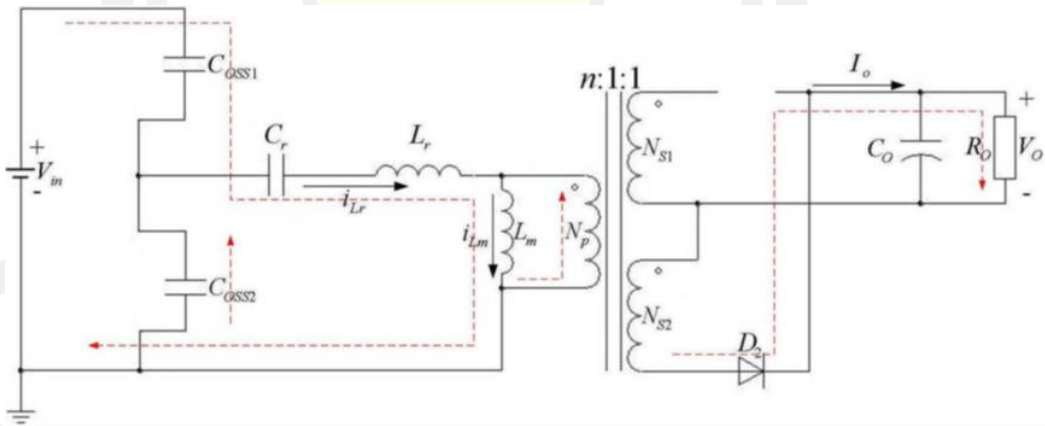




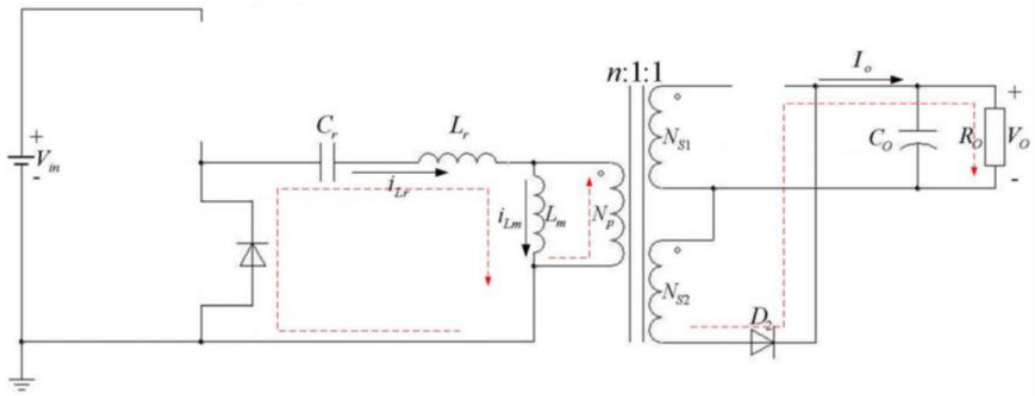
Phase2 ( $t_1 < t < t_2$ )



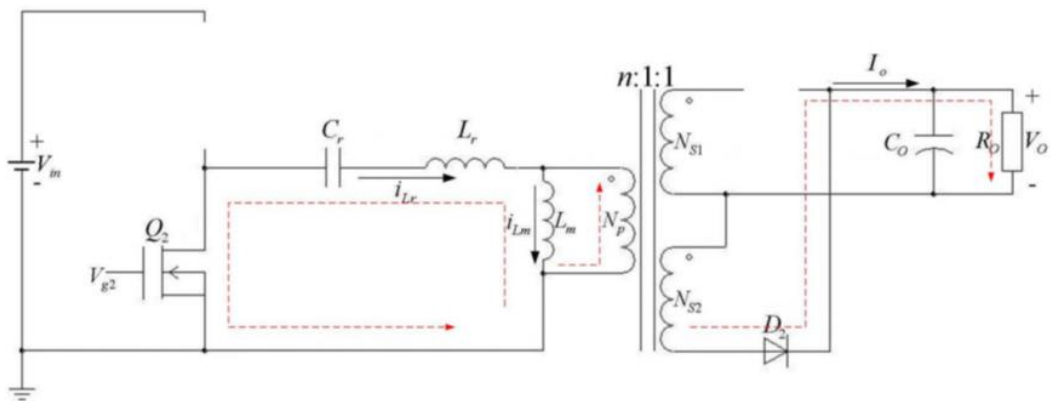
Phase3 ( $t_2 < t < t_3$ )



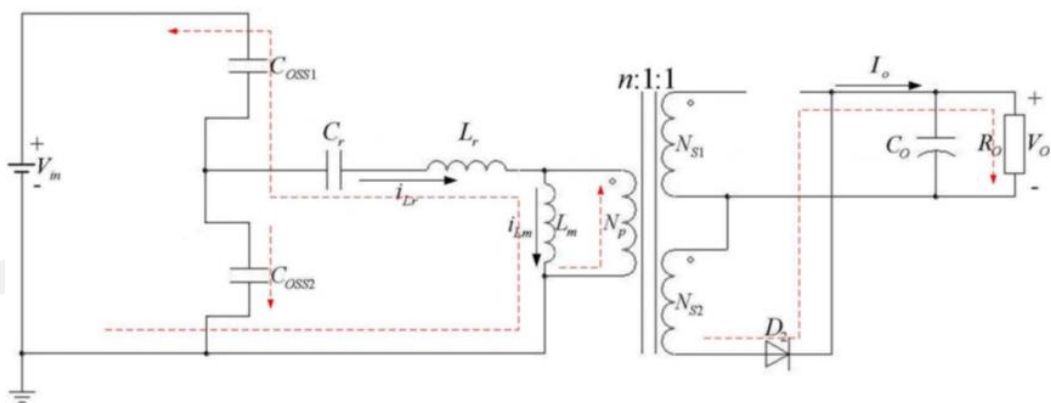
Phase4 ( $t_3 < t < t_4$ )



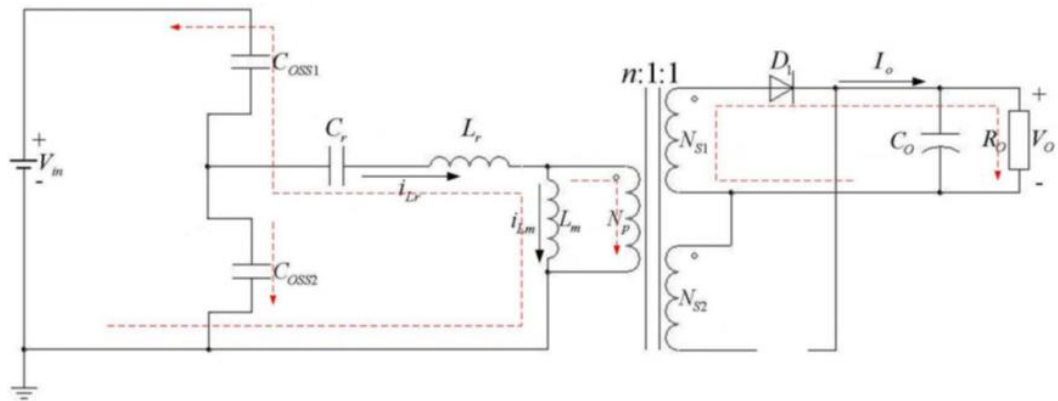
Phase5 (  $t_4 < t < t_5$  )



Phase6 (  $t_5 < t < t_6$  )



Phase7 (  $t_6 < t < t_7$  )



Phase8 (  $t_7 < t < t_8$  )

**Figure 11** LLC resonant circuit Operation sequence with  $f > f_s$

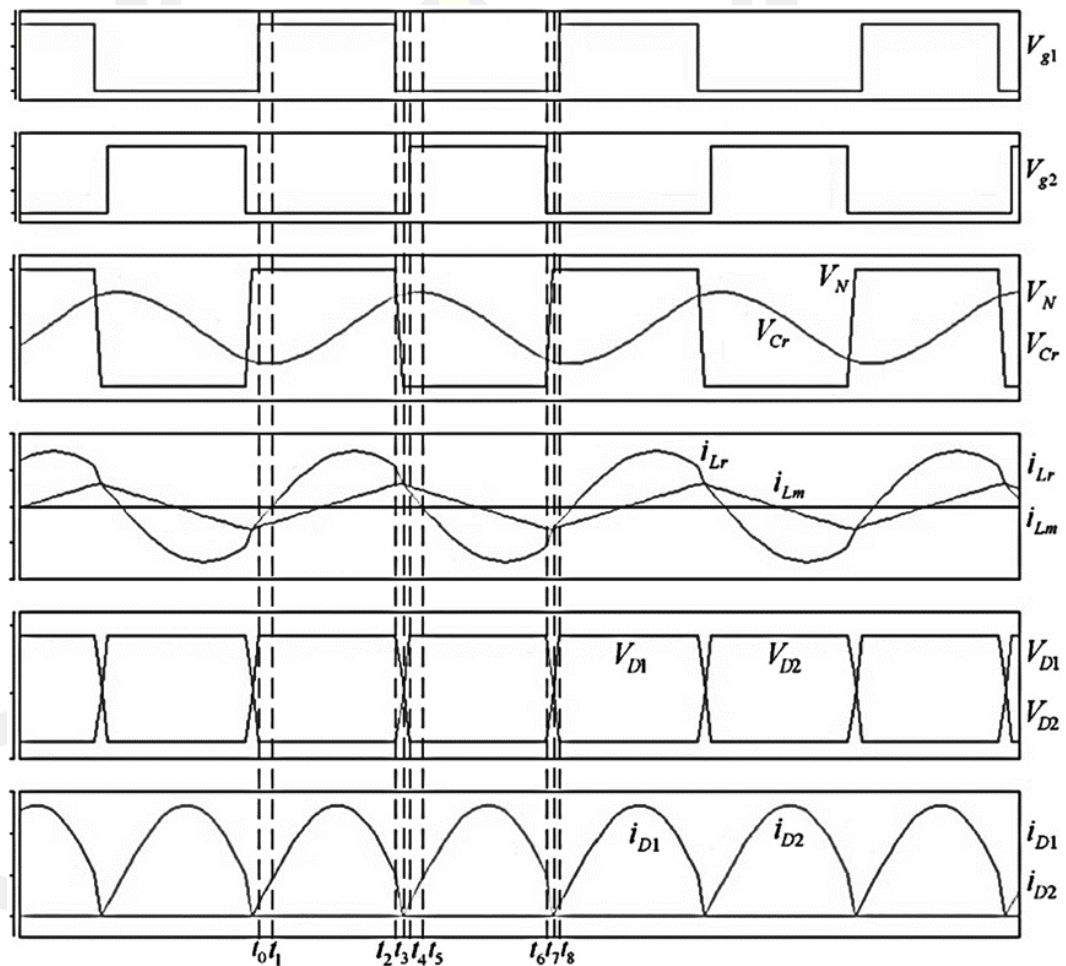


**Figure 12** LLC resonant circuit Operation waveforms with  $f > f_s$

Phase 1 (  $t_0 < t < t_1$  )

This phase is similar to the one at  $f_m < f < f_s$ , where the current in the resonant inductor  $L_r$  flows through the body diode of Q1, creating the conditions for the ZVS conduction of Q1. The rectifier diode D1 conducts,  $L_m$  is clamped by the output voltage, and only  $L_r$  and  $C_r$  are involved in resonance.

The phase 1 operating state ends when the resonant current  $i_{Lr}$  rises to 0.

Phase 2 (  $t_1 < t < t_2$  )

At  $t_1$ , Q1 turns on, rectifier diode D1 turns on, and  $L_m$  is clamped by the output voltage and does not participate in resonance. At this phase, the whole circuit resembles a series resonant circuit with resonant inductor  $L_r$  and resonant capacitor  $C_r$ .

When Q1 is turned off, the phase 2 operating state ends.

Phase 3 (  $t_2 < t < t_3$  )

At  $t_2$ , Q1 and Q2 turn off and enter the dead time. The current flowing through  $L_r$  and  $L_m$  charges Q1's parasitic capacitor  $C_{oss1}$  and discharges Q2's parasitic capacitor  $C_{oss2}$ . Because the switching period is shorter than the resonant period of resonant capacitor  $C_r$  and resonant inductor  $L_r$ , when Q1 turns off, the resonant current has not yet completed half a cycle.

Therefore, the current in  $L_r$  is larger than the current in  $L_m$ , and the difference flows through the primary side of the transformer, the rectifier diode D1 is still on, and  $L_m$  is clamped by the output voltage.

When  $C_{oss2}$  is discharged, the body diode of Q2 is turned on, and the working state of phase 3 is finished at this time.

Phase 4 (  $t_3 < t < t_4$  )

At this time  $i_{Lr}$  continues to decrease to less than  $i_{Lm}$ , the difference between the two flows through the primary side of the transformer, the polarity of the primary side of the transformer becomes up negative and down positive, the rectifier diode D2 begins to conduct,  $L_m$  is clamped by the output voltage.

The working process of the latter half-cycle converter is similar to that of the first half-cycle, so the subsequent half-cycle working process will not be described in detail.

### Design of the LLC Resonant Converter Parameters

SYMBOL	PARAMETER	MINIMUM	NOMINAL	MAXIMUM	UNIT
VIN	DC input voltage	320	385	395	V DC
Vout	Output voltage	45	48	52	V DC
Pout	Output power			528	Watt
$\eta$	Targeted efficiency		95%		
fsw	Switching frequency		116 k		Hz

**Table 2** Target design parameters for the LLC stage

From the nominal input voltage  $V_{in\_nom}$ , the transformer turns ratio can be determined.

$$n = \frac{V_{in\_nom}}{2 \times (V_o + V_F)} \quad (7)$$

The required gain at maximum and minimum input voltage can be determined using the following equations.

$$M_{min} = \frac{n \times (V_o + V_F)}{V_{in\_max}/2} \quad (8)$$

$$M_{max} = \frac{n \times (V_o + V_F)}{V_{in\_min}/2} \quad (9)$$

$M_{min} = 0.5367$  and  $M_{max} = 0.6625$  can be obtained.

Calculate the equivalent load resistance:

$$R_e = \frac{8n^2}{\pi^2} \times \frac{V_o}{I_o} \quad (10)$$

The resonant circuit is composed of resonant capacitor  $C_r$  and resonant inductor  $L_r$ . The resonance parameters can be calculated from the following equations:

$$C_r = \frac{1}{2\pi Q_e f_r R_e} \quad (11)$$

$$L_r = \frac{1}{(2\pi f_r)^2 C_r} \quad (12)$$

The magnetizing inductance can be calculated as:

$$L_m = m \times L_r \quad (13)$$

Finally get  $C_r = 2 \times 47 \text{ nF}$ ,  $L_r = 20 \mu\text{H}$ .

In a real transformer, the resonant inductance can be integrated into the transformer, and the primary coil inductance is equal to:

$$L_p = L_m + L_r \quad (14)$$

For an integrated transformer, the actual turns ratio of the transformer should be calculated according to the following formula.

$$n_{real} = n \sqrt{\frac{L_r + L_m}{L_m}} \quad (15)$$

The secondary and primary side turns can be calculated according to the following formula.

$$N_s = \frac{V_o + V_F}{4f_{min} \times \Delta B \times A_e} \quad (16)$$

$$N_p = N_s \times n_{real} \quad (17)$$

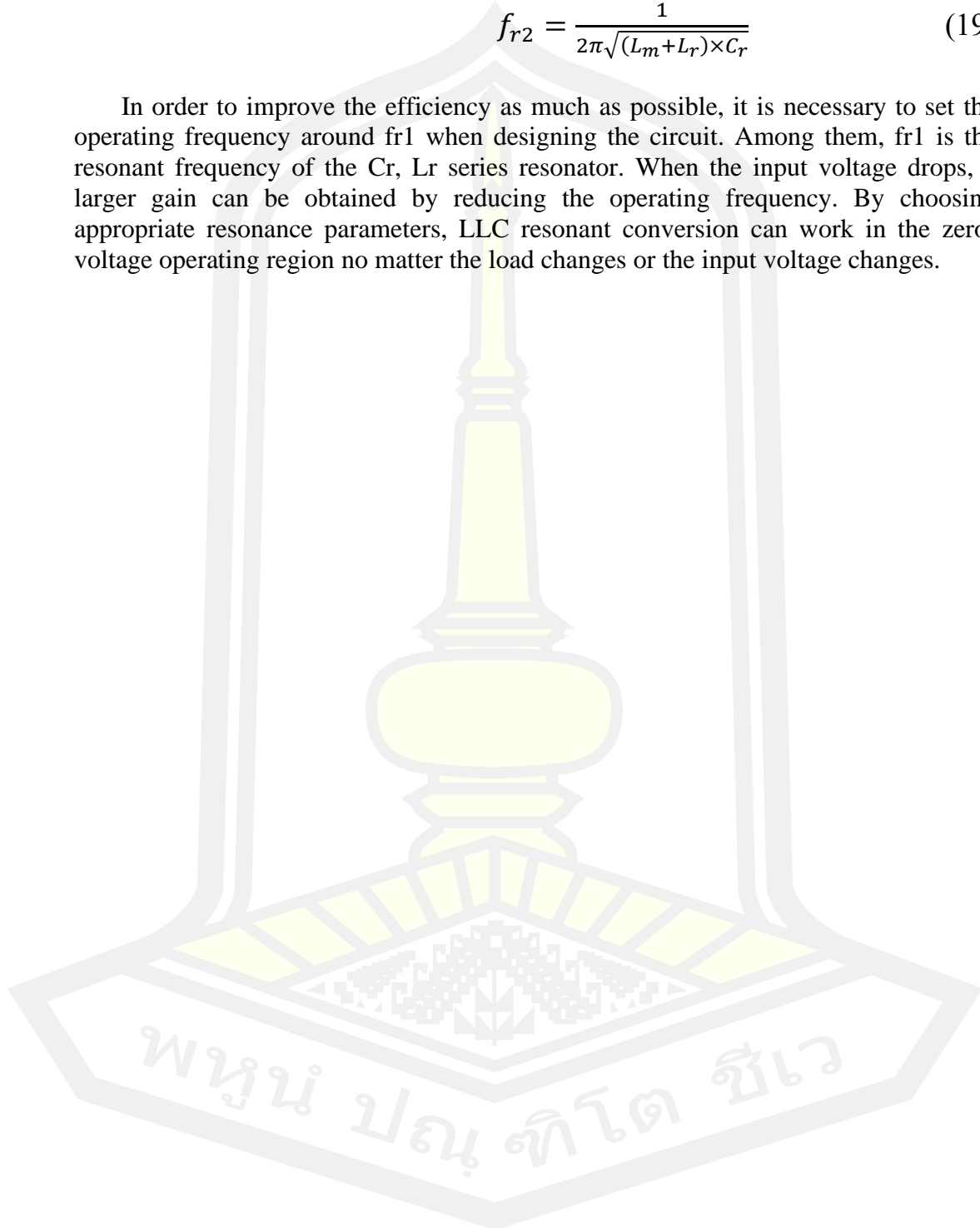
Finally get  $N_p = 18:5$ .

The DC characteristics of LLC resonant conversion are divided into the zero-voltage operating region and zero-current operating region. This transformation has two resonant frequencies. One is the resonance point of  $L_r$  and  $C_r$ , and the other is determined by  $L_m$ ,  $C_r$ , and load conditions. The heavier the load, the higher the resonant frequency. The calculation formulas of these two resonance points are as follows[50]:

$$f_{r1} = \frac{1}{2\pi\sqrt{L_r \times C_r}} \quad (18)$$

$$f_{r2} = \frac{1}{2\pi\sqrt{(L_m + L_r) \times C_r}} \quad (19)$$

In order to improve the efficiency as much as possible, it is necessary to set the operating frequency around  $f_{r1}$  when designing the circuit. Among them,  $f_{r1}$  is the resonant frequency of the  $C_r, L_r$  series resonator. When the input voltage drops, a larger gain can be obtained by reducing the operating frequency. By choosing appropriate resonance parameters, LLC resonant conversion can work in the zero-voltage operating region no matter the load changes or the input voltage changes.



## CHAPTER IV

### TEST RESULTS AND DISCUSSIONS

This chapter presents the test results to confirm and validate the feasibility of the proposed study. The following steps illustrate the simulation process performed using the simulation software (Synopsys Saber2012) and present a discussion of the results.

#### Simulation Models

Figure.13 and Figure 14 show the simulation circuit of Totem-pole bridgeless PFC and LLC. Table 3 shows the key parameter comparison between the GaN HEMT (LMG3410R070) [51] and the Si MOS device (IPB60R070CFD7)[52].

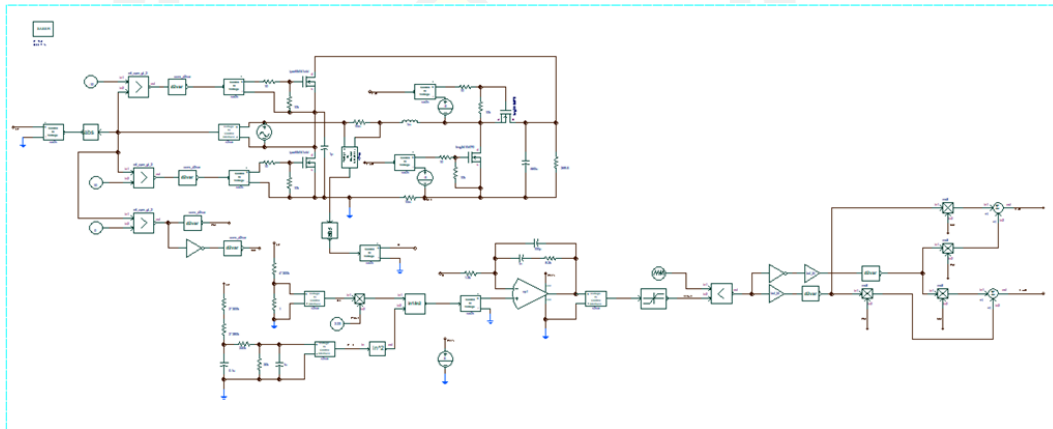


**Figure 13** Totem-pole bridgeless PFC Simulation Circuit

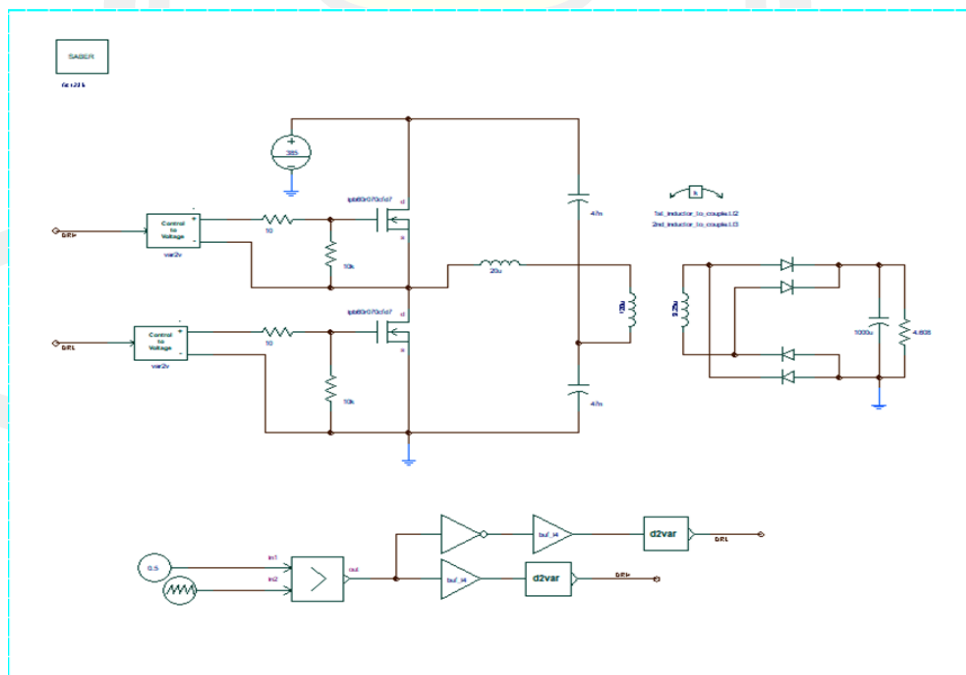


**Figure 14** LLC Simulation Circuit

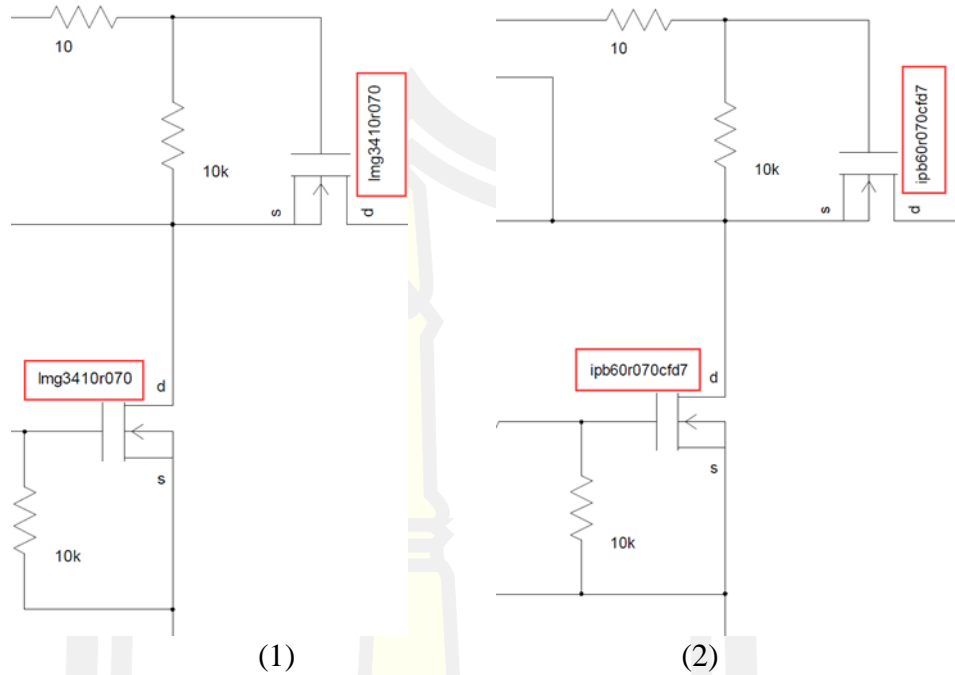


**Figure 15** simulation schematic diagram details comparison, (1) GaN HEMT (LMG3410R070), (2) Si MOS (IPB60R070CFD7)

Symbol	Parameters	Si CoolMOSCFD7	GaN HEMT	Unit
		IPB60R070CFD7	LMG3410R070	
VDS	Drain-to-Source Voltage	650	600	V
RDS(ON)	Drain-to-Source On Resistance	70	70	mΩ
QG	Total Gate Charge	67	4.5	nC
CO(ER)	Effective Output Capacitance Energy Related	96	95	pF
CO(TR)	Effective Output Capacitance Time Related	990	145	pF

**Table 3** Comparison of key parameters between GaN HEMT (LMG3410R070) and Si MOS device (IPB60R070CFD7).

When simulating GaN HEMT and Si MOS devices, as shown in Figure 15, it is only necessary to replace Q3 and Q4, and all other parameters of the simulation circuit remain the same. In the Totem-pole bridgeless PFC simulation, the GaN HEMT simulation uses a switching frequency of 500KHz, and the Si MOS device uses a switching frequency of 100KHz.

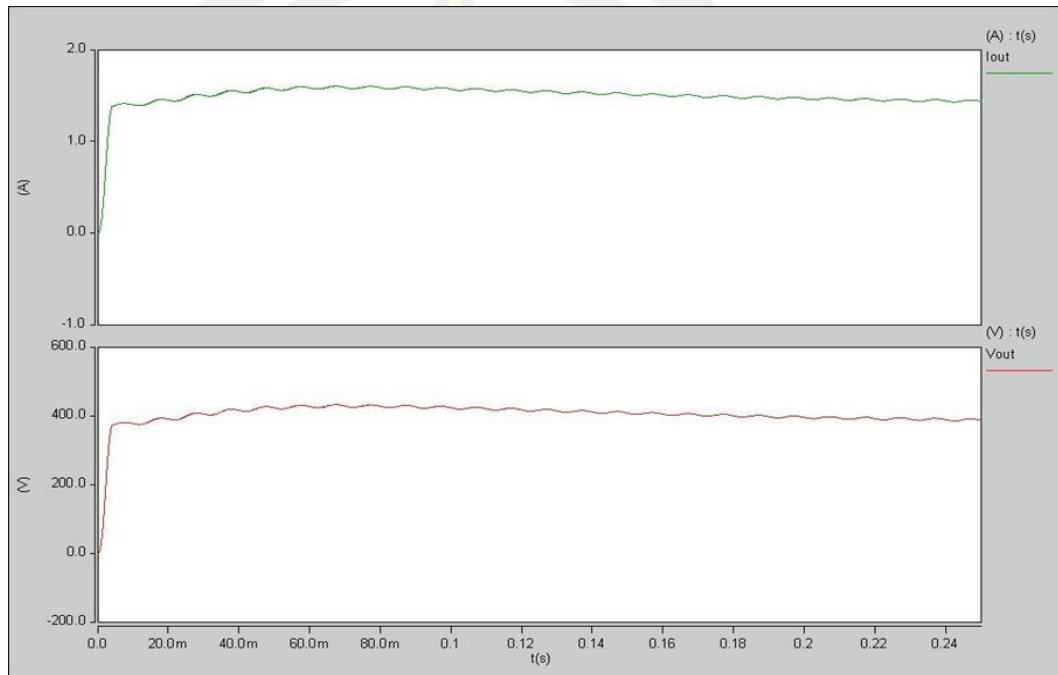
### Simulated Results

To verify the performance comparison of the proposed GaN-based HEMT with silicon-based Totem-pole bridgeless PFC Circuit and LLC resonant circuit, the following tests were performed.

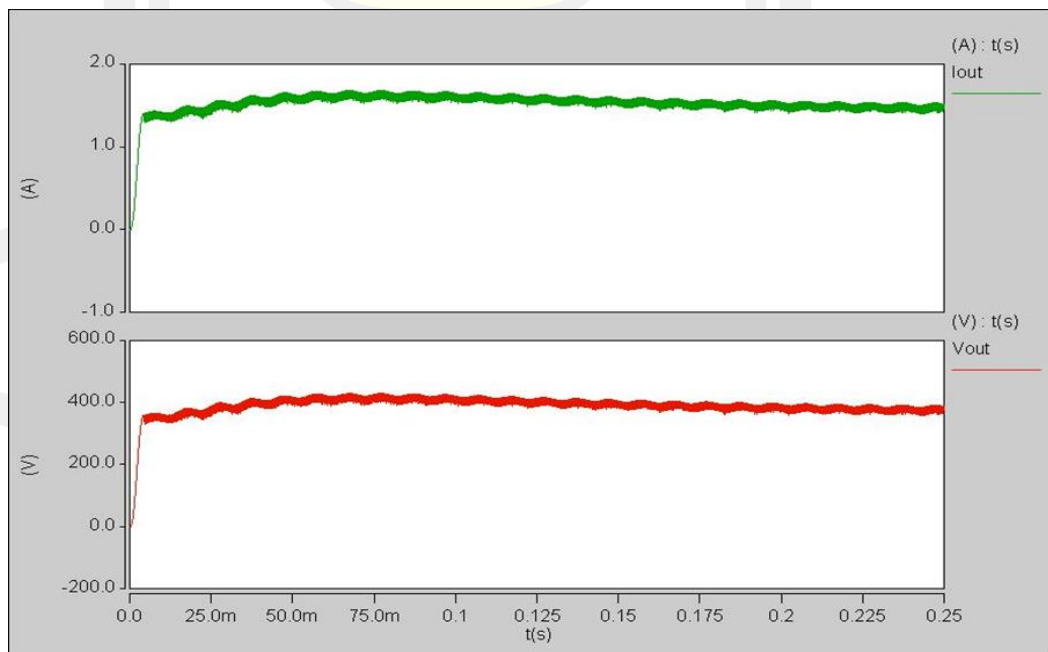


### 1. Comparison of the Outputs

Comparison of the Totem-pole bridgeless PFC Circuit Outputs, Figure 16 is the output voltage and current waveforms using the GaN HEMT device, Figure 17 is the output voltage and current waveform using the Si MOS device, it can be seen that the output of the Totem-pole bridgeless PFC circuit using the GaN HEMT device is more stable.

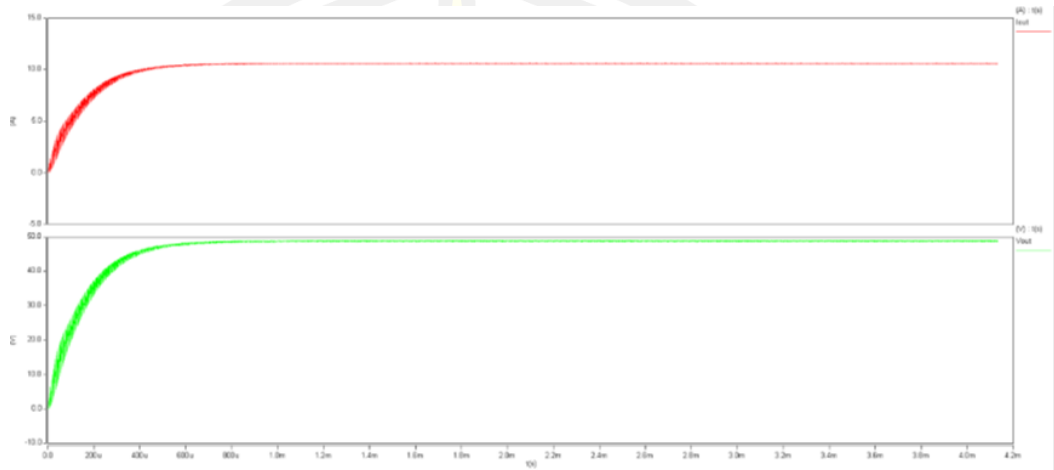


**Figure 16** Totem-pole bridgeless PFC Circuit output voltage and current waveforms using the GaN HEMT device

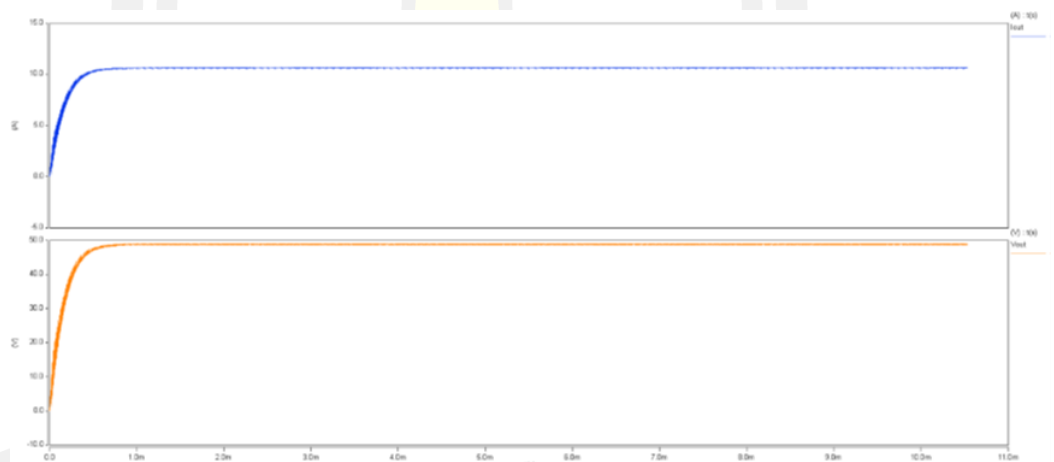


**Figure 17** Totem-pole bridgeless PFC Circuit output voltage and current waveform using the Si MOS device

Comparison of LLC resonant circuit output, Figure 18 is the output voltage and current waveforms using GaN HEMT devices, Figure 19 is the output voltage and current waveforms using Si MOS devices,  $V_{rms}=48.795$  V,  $I_{rms}=10.589$  A when using GaN HEMT devices,  $V_{rms}=48.74$  V and  $I_{rms}=10.577$  A when using Si MOS devices, it can be seen that the two types of output waveforms in the LLC resonant circuit are basically the same when the resonant frequency is not high.



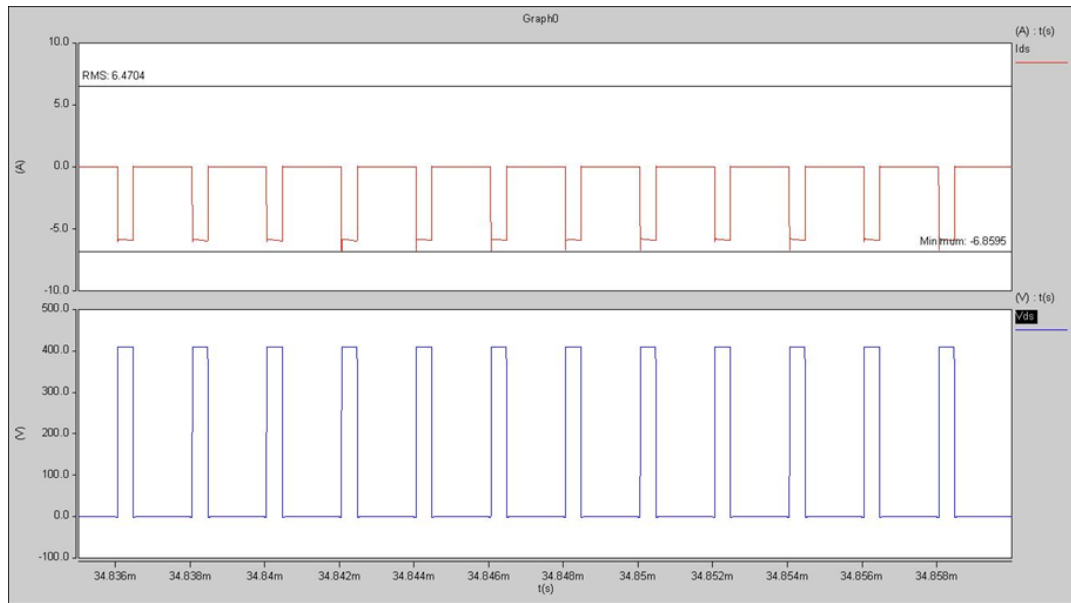
**Figure 18** LLC Resonant Circuit output voltage and current waveform using the GaN HEMT device



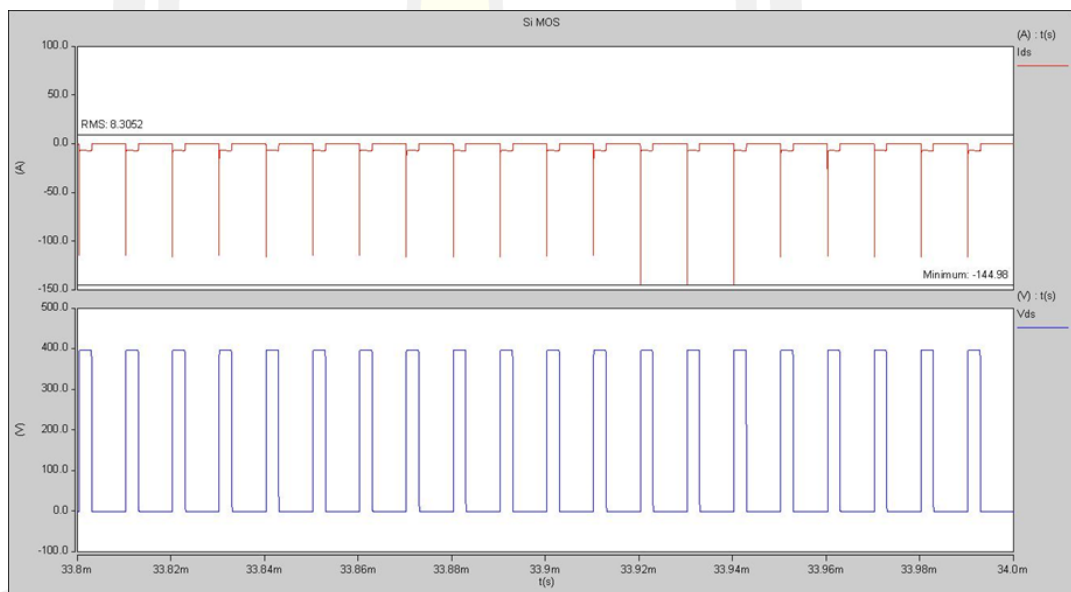
**Figure 19** LLC Resonant Circuit output voltage and current waveform using the Si MOS device

## 2. Comparison of Voltage and Current Stresses on Semiconductor Devices

Figure 20 is the Totem-pole bridgeless PFC Circuit GaN HEMT device voltage and current, Figure 21 is the Totem-pole bridgeless PFC Circuit Si MOS device voltage and current, since GaN has no body diode problem, it can be seen that the peak reverse recovery current of the PFC circuit of the GaN-based device is  $-6.8595$  A<sub>peak</sub>, while that of the Si-based device is  $-144.98$  A<sub>peak</sub>. This shows that GaN-based devices provide less voltage and current stress on circuit elements than Si-based devices.

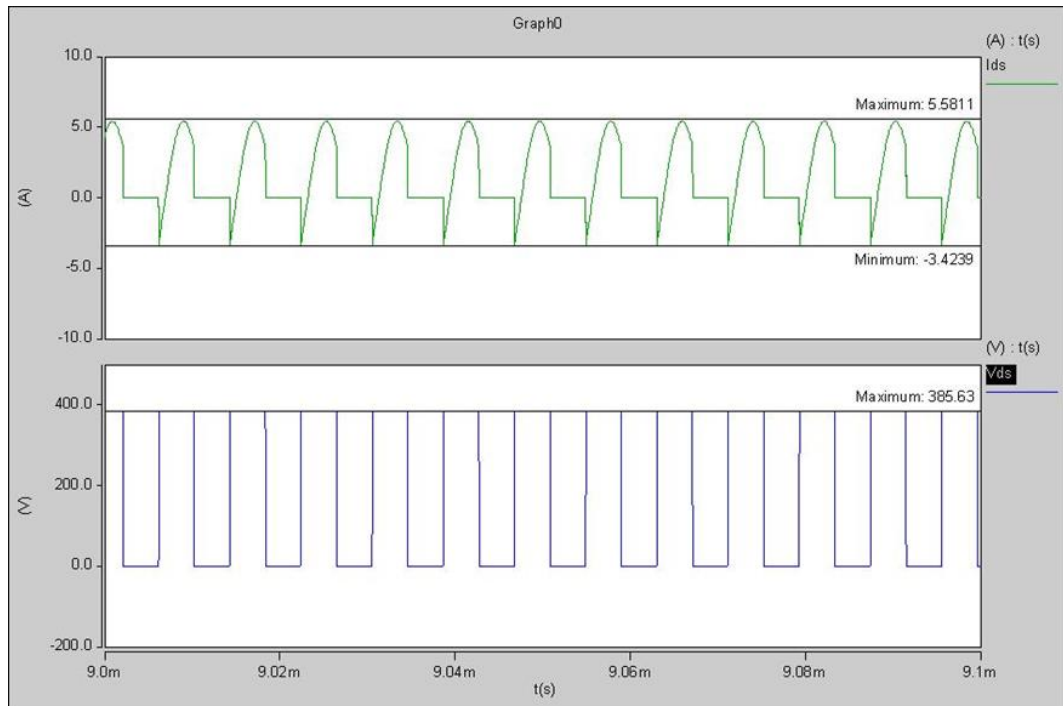


**Figure 20** Totem-pole bridgeless PFC Circuit GaN HEMT device voltage and current

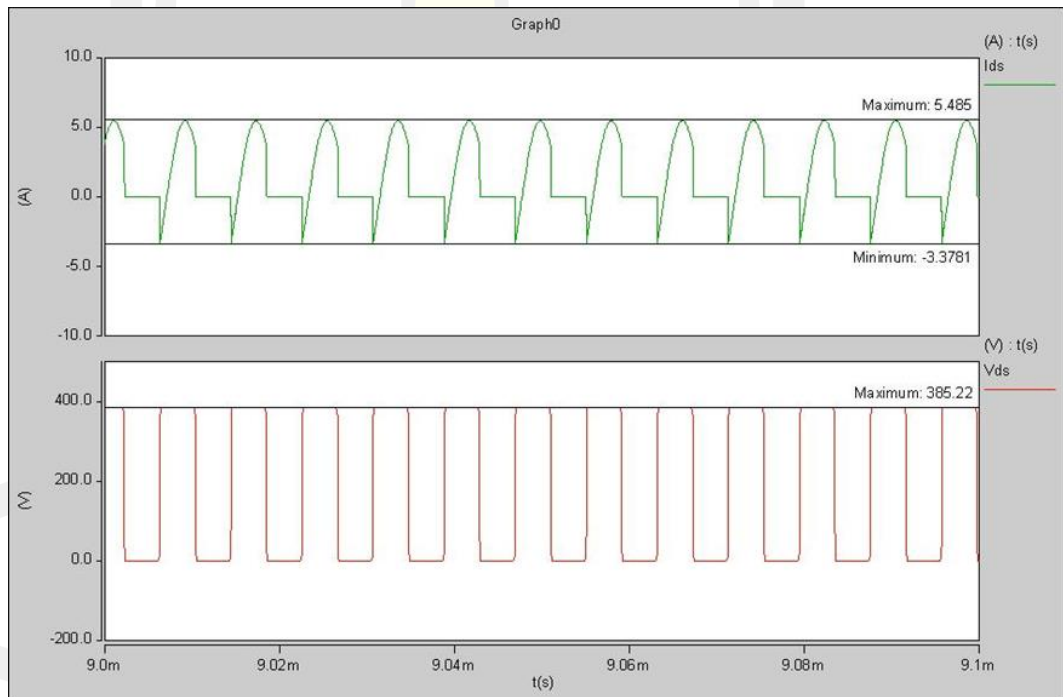


**Figure 21** Totem-pole bridgeless PFC Circuit Si MOS device voltage and current

Figure 22 is the voltage and current of the GaN HEMT device in the Totem-pole bridgeless PFC circuit, and Figure 23 is the voltage and current of the Si MOS device in the Totem-pole bridgeless PFC circuit. When using the GaN HEMT device,  $V_{\text{peak}}=385.63$  V,  $I_{\text{peak}}=5.5811$  A, when using the Si MOS device  $V_{\text{peak}}=385.22$  V,  $I_{\text{peak}}=5.485$  A, it can be seen that in the LLC resonant circuit, the current and voltage stress of GaN HEMT and Si MOS are basically the same.



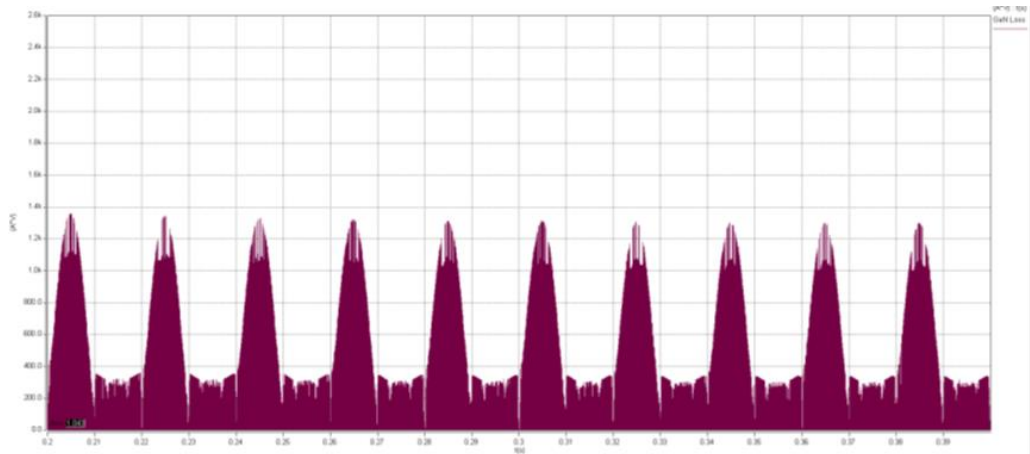
**Figure 22** LLC Resonant Circuit GaN HEMT device voltage and current



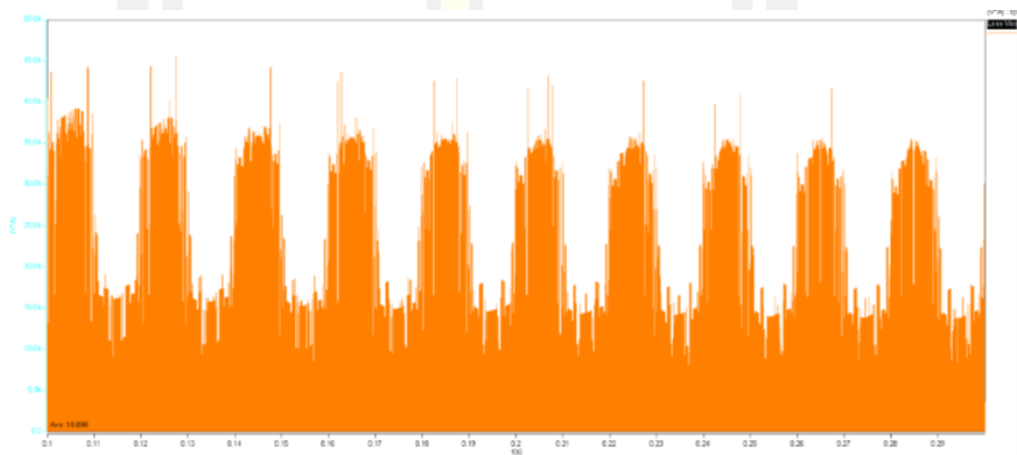
**Figure 23** LLC Resonant Circuit Si MOS device voltage and current

### 3. Semiconductor device loss comparison

Figure 24 is the Loss of Totem-pole bridgeless PFC Circuit GaN HEMT device, its average loss is 1.043 W. Figure 25 is the Loss of Totem-pole bridgeless PFC Circuit Si MOS device, its average loss is 18.898 W. The loss of Si MOS device is 18.12 times that of GaN HEMT device.



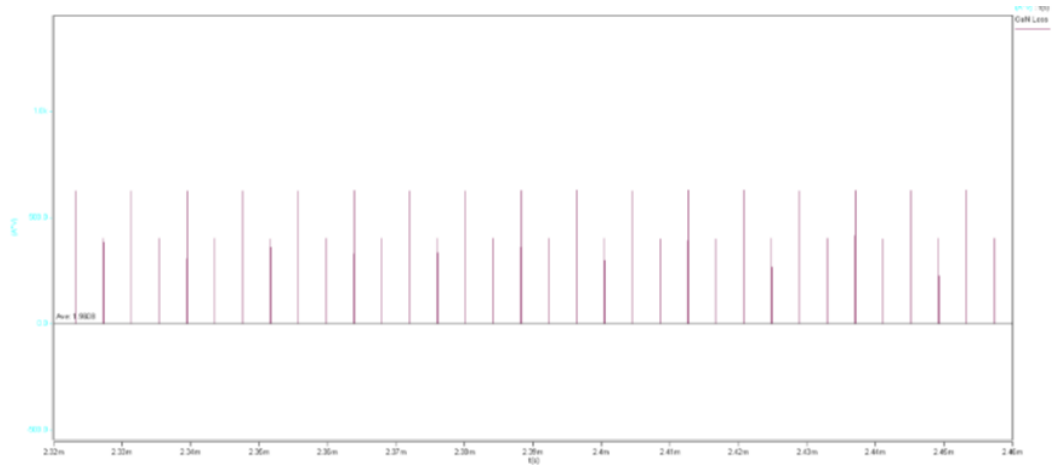
**Figure 24** Loss of Totem-pole bridgeless PFC Circuit GaN HEMT device



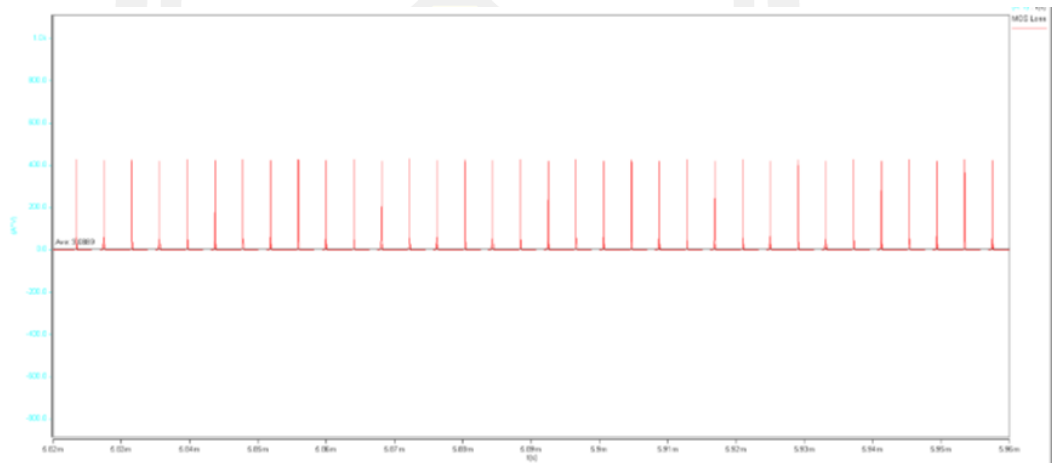
**Figure 25** Loss of Totem-pole bridgeless PFC Circuit Si MOS device

Figure 26 is the Loss of LLC Resonant Circuit GaN HEMT device, its average loss is 1.9608 W. Figure 27 is the Loss of LLC Resonant Circuit Si MOS device, its average loss is 3.0889 W. When LLC uses GaN as the main switching device, its loss reduction effect is not as obvious as that of the PFC stage, mainly because LLC is a soft switching topology, and its switching loss is already very small. Compared with GaN devices, the Si MOS used The  $R_{dson}$  of the device is also  $70\text{m}\Omega$ . Therefore, compared with the PFC stage, the loss of the GaN HEMT device is only 63.5% lower than that of the Si MOS device.

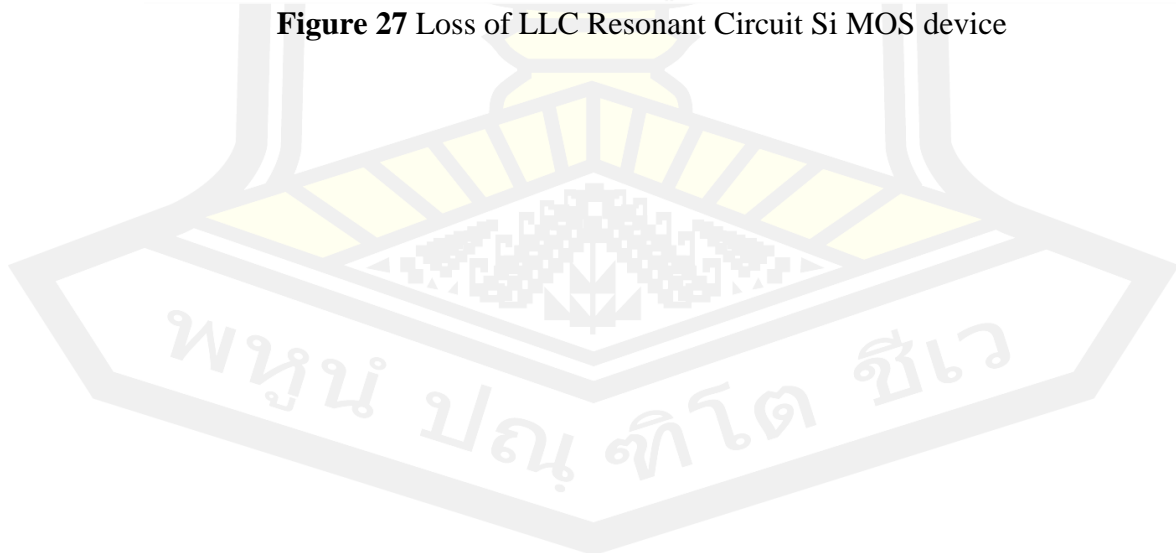
พหุบัณฑิต ชีวะ



**Figure 26** Loss of LLC Resonant Circuit GaN HEMT device



**Figure 27** Loss of LLC Resonant Circuit Si MOS device



## CHAPTER V

### CONCLUSIONS

This chapter presents the conclusions drawn from the simulations in Chapter 4, along with recommendations and future work.

#### Conclusions

In Section 1. Comparison of the Outputs, it can be seen that the output of the Totem-pole bridgeless PFC+LLC power supply based on GaN devices is more stable. And because the GaN HEMT device operates at a higher frequency, the required inductor volume is smaller, according to the calculation in Chapter 3, when the GaN HEMT operates at a frequency of 500 kHz and the Si MOS operates at a frequency of 100 kHz, the inductance volume required by the GaN device circuit is only 20% of that of the Si MOS device circuit, and the overall volume can be smaller.

In Section 2. Comparison of Voltage and Current Stresses on Semiconductor Devices, it can be seen that due to the slow recovery of the body diode of MOS, a large current inversion pulse will be generated, and the peak current will be extremely large, which will cause great danger to the circuit, while GaN HEMT has no body diode, so there is no this problem.

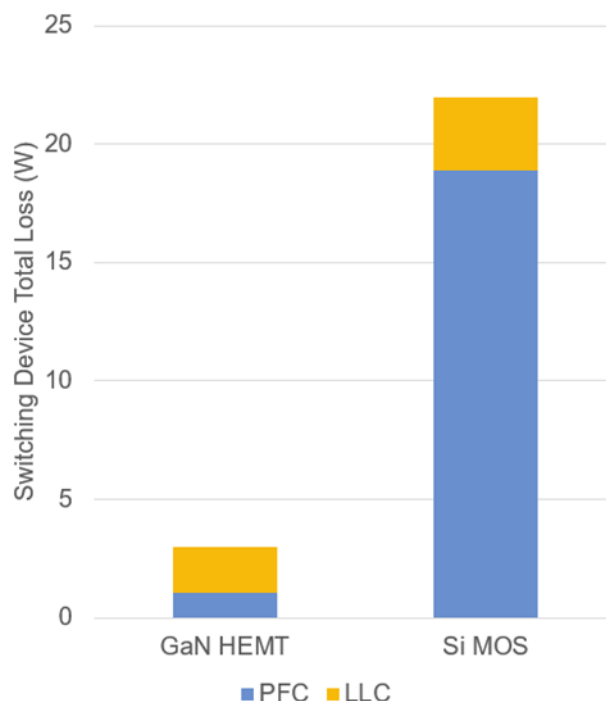


**Figure 28** Switching Device Total Loss Comparison

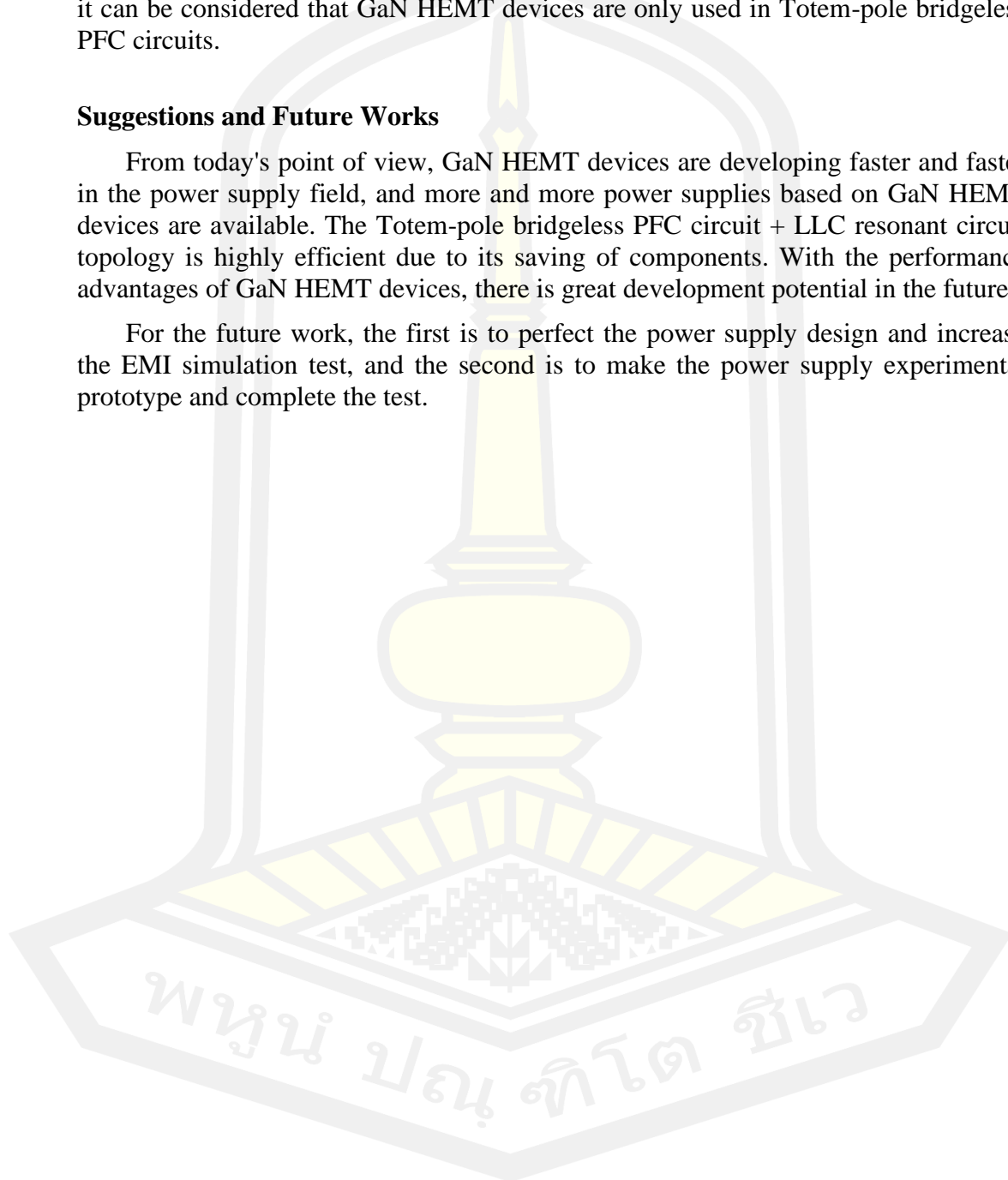
In Section 3. Semiconductor device loss comparison, we can see the loss comparison of GaN HEMT device and Si MOS device in Totem-pole bridgeless PFC circuit and LLC resonant circuit. The losses of Si MOS devices are very high,

reaching an average loss of 18.898 W, while the average loss of GaN devices operating at 500kHz is only 1.043 W. In the LLC resonant circuit, although the loss of the GaN HEMT device (1.9608 W) can still reduce the loss by 1/3 compared to the loss of the Si MOS device (3.0889 W), the loss is compared to the total output. It is not high. Considering the current cost gap between GaN HEMT and Si MOS devices, it can be considered that GaN HEMT devices are only used in Totem-pole bridgeless PFC circuits.

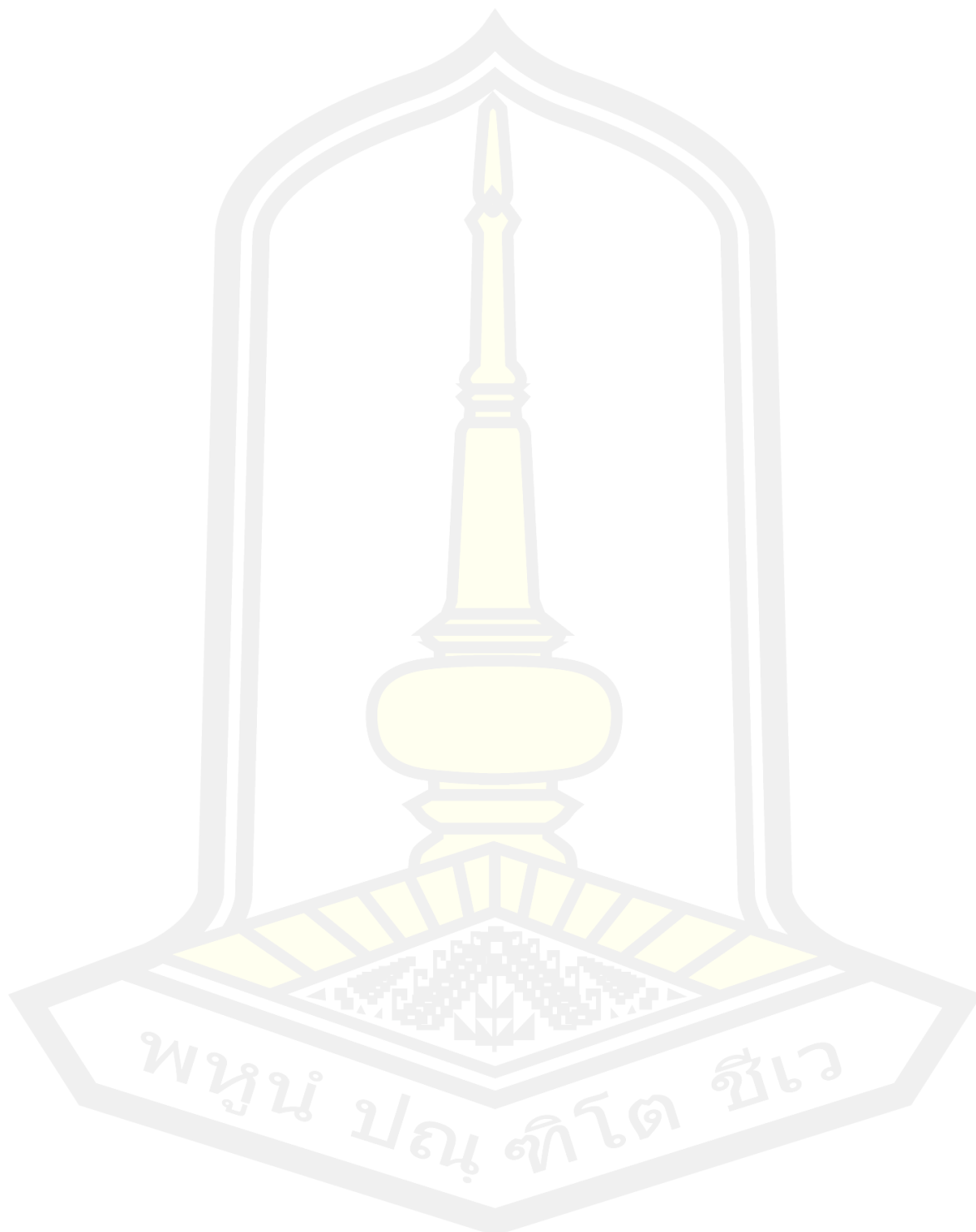
### **Suggestions and Future Works**

From today's point of view, GaN HEMT devices are developing faster and faster in the power supply field, and more and more power supplies based on GaN HEMT devices are available. The Totem-pole bridgeless PFC circuit + LLC resonant circuit topology is highly efficient due to its saving of components. With the performance advantages of GaN HEMT devices, there is great development potential in the future.

For the future work, the first is to perfect the power supply design and increase the EMI simulation test, and the second is to make the power supply experimental prototype and complete the test.





**REFERENCES**

## REFERENCES

- [1] C. C. R. Yeh, C. C. J. Wong, W. W. V. Chang, and C. C. S. Lai, "Labor Displacement in Artificial Intelligence Era: A Systematic Literature Review," (in English), *Taiwan J. East Asian Stud.*, Review vol. 17, no. 2, pp. 25-75, Dec 2020, doi: 10.6163/tjeas.202012\_17(2).0002.
- [2] I. F. o. R. (IFR), Executive Summary WR Service Robots 2021.
- [3] c. Shi. "家用服务机器人分析." <https://robot.ofweek.com/2021-11/ART-8321200-8420-30533621.html> (accessed).
- [4] "移动机器人迅速纳入主流，加速渗透多个行业." <https://robot.ofweek.com/2021-11/ART-8321200-8400-30535774.html> (accessed).
- [5] "World Robotics 2021 – Service Robots report released." <https://ifr.org/ifr-press-releases/news/service-robots-hit-double-digit-growth-worldwide> (accessed).
- [6] M. Li, Z. Yang, Y. Ding, Y. Z. Li, and I. Destech Publicati, "Study on Charging Load Under Different Charging Modes of Electric Vehicles," in 4th International Conference on Materials Engineering for Advanced Technologies (ICMEAT), London, ENGLAND, Jun 27-28 2015, LANCASTER: Destech Publications, Inc, 2015, pp. 670-673. [Online]. Available: <Go to ISI>://WOS:000361105400149. [Online]. Available: <Go to ISI>://WOS:000361105400149
- [7] T. Deguchi, T. Kikuchi, M. Arai, K. Yamasaki, and T. Egawa, "High On/Off current ratio p-InGaN/AlGaIn/GaN HEMTs," *IEEE Electron Device Lett.*, Article vol. 33, no. 9, pp. 1249-1251, 2012, Art no. 6248156, doi: 10.1109/LED.2012.2204854.
- [8] G. Greco, F. Iucolano, and F. Roccaforte, "Review of technology for normally-off HEMTs with p-GaN gate," *Materials Science in Semiconductor Processing, Review* vol. 78, pp. 96-106, 2018, doi: 10.1016/j.mssp.2017.09.027.
- [9] N. Kim, J. Yu, W. Zhang, R. Li, M. Wang, and W. T. Ng, "Current Trends in the Development of Normally-OFF GaN-on-Si Power Transistors and Power Modules: A Review," *Journal of Electronic Materials*, Article vol. 49, no. 11, pp. 6829-6843, 2020, doi: 10.1007/s11664-020-08284-7.
- [10] M. Kuzuhara and H. Tokuda, "Low-loss and high-voltage III-nitride transistors for power switching applications," *IEEE Transactions on Electron Devices*, Article vol. 62, no. 2, pp. 405-413, 2015, Art no. 6967816, doi: 10.1109/TED.2014.2359055.
- [11] M. Meneghini, G. Meneghesso, and E. Zanoni, "Power GaN Devices," Cham: Springer International Publishing, 2017.
- [12] U. K. Mishra, P. Parikh, and Y. F. Wu, "AlGaIn/GaN HEMTs - An overview of device operation and applications," *Proceedings of the IEEE*, Article vol. 90, no. 6, pp. 1022-1031, 2002, doi: 10.1109/JPROC.2002.1021567.
- [13] R. Quay, Gallium nitride electronics. Springer Science & Business Media, 2008.

- [14] F. Ren and J. C. Zolper, *Wide energy bandgap electronic devices*. World Scientific, 2003.
- [15] P. J. Kong, S. Wang, and F. C. Lee, "Common mode EMI noise suppression for bridgeless PFC converters," (in English), *IEEE Trans. Power Electron.*, Article; Proceedings Paper vol. 23, no. 1, pp. 291-297, Jan 2008, doi: 10.1109/tpel.2007.911877.
- [16] K. Mainali and R. Oruganti, "Conducted EMI Mitigation Techniques for Switch-Mode Power Converters: A Survey," *IEEE Trans. Power Electron.*, vol. 25, no. 9, pp. 2344-2356, Sep 2010, doi: 10.1109/tpel.2010.2047734.
- [17] R. A. Siddique, R. Khandekar, P. Ksiazek, and J. Wang, "Investigation of Zero-Crossing Common-Mode Noise and Current Spike in GAN Based Totem-Pole PFC," in *2018 IEEE Canadian Conference on Electrical & Computer Engineering (CCECE)*, 13-16 May 2018 2018, pp. 1-5, doi: 10.1109/CCECE.2018.8447724.
- [18] V. Vlatkovic, D. Borojevic, and F. C. Lee, "Input filter design for power factor correction circuits," *IEEE Trans. Power Electron.*, vol. 11, no. 1, pp. 199-205, Jan 1996, doi: 10.1109/63.484433.
- [19] L. Xue, Z. Shen, D. Boroyevich, and P. Mattavelli, "GaN-based high frequency totem-pole bridgeless PFC design with digital implementation," in *2015 IEEE Applied Power Electronics Conference and Exposition (APEC)*, 15-19 March 2015 2015, pp. 759-766, doi: 10.1109/APEC.2015.7104435.
- [20] D. Zhang, Y. Luo, B. Jin, and Y. Sun, "The Design of 100 W Switching Power Supply APFC Based on L6563," in *2012 Asia-Pacific Power and Energy Engineering Conference*, 27-29 March 2012 2012, pp. 1-4, doi: 10.1109/APPEEC.2012.6307400.
- [21] G. K. Andersen and F. Blaabjerg, "Current programmed control of a single-phase two-switch buck-boost power factor correction circuit," *IEEE Trans. Ind. Electron.*, vol. 53, no. 1, pp. 263-271, 2006, doi: 10.1109/TIE.2005.862252.
- [22] Y. Liyu et al., "Modeling and characterization of a 1 KW CCM PFC converter for conducted EMI prediction," in *Nineteenth Annual IEEE Applied Power Electronics Conference and Exposition, 2004. APEC '04.*, 22-26 Feb. 2004 2004, vol. 2, pp. 763-769 vol.2, doi: 10.1109/APEC.2004.1295909.
- [23] D. M. Mitchell, "AC-DC converter having an improved power factor," Patent U.S. Patent 4 412 277, 1983.
- [24] F. S. I. Barbi., "High power factor rectifier with reduced conduction and commutation losses," Jun. 1999 1999, vol. 8, pp. pp. 8.1.1– 8.1.5.
- [25] L. Xue., Z. Shen., D. Boroyevich., and P. Mattavelli., "GaN-based high frequency totem-pole bridgeless PFC design with digital implementation," in *2015 IEEE Applied Power Electronics Conference and Exposition (APEC)*, 15-19 March 2015 2015, pp. 759-766, doi: 10.1109/APEC.2015.7104435.
- [26] L. Huber, Y. Jang, and M. M. Jovanović, "Performance evaluation of bridgeless PFC boost rectifiers," *IEEE Trans. Power Electron.*, Article vol. 23, no. 3, pp. 1381-1390, 2008, doi: 10.1109/TPEL.2008.921107.
- [27] Y. Jang and M. M. Jovanovic, "A Bridgeless PFC Boost Rectifier With Optimized Magnetic Utilization," *IEEE Trans. Power Electron.*, vol. 24, no. 1, pp. 85-93, 2009, doi: 10.1109/TPEL.2008.2006054.

- [28] Z. Sun and S. Bae, "Multiple-Input Soft-Switching Step-up/down Converter for Renewable Energy Systems," in 2018 7th International Conference on Renewable Energy Research and Applications (ICRERA), 14-17 Oct. 2018 2018, pp. 632-636, doi: 10.1109/ICRERA.2018.8567017.
- [29] G. Yilei, H. Lijun, C. Shijie, D. Yu, L. Zhengyu, and Q. Zhaoming, "Research on control type soft switching converters," in 2004 IEEE 35th Annual Power Electronics Specialists Conference (IEEE Cat. No.04CH37551), 20-25 June 2004 2004, vol. 2, pp. 1470-1475 Vol.2, doi: 10.1109/PESC.2004.1355641.
- [30] W. Zhang, F. Wang, D. J. Costinett, L. M. Tolbert, and B. J. Blalock, "Investigation of Gallium Nitride Devices in High-Frequency LLC Resonant Converters," *IEEE Trans. Power Electron.*, vol. 32, no. 1, pp. 571-583, 2017, doi: 10.1109/TPEL.2016.2528291.
- [31] W. Zhang, Y. Cui, F. Wang, L. M. Tolbert, B. J. Blalock, and D. J. Costinett, "Investigation of Gallium Nitride devices benefits on LLC resonant DC-DC converter," in 2015 IEEE Applied Power Electronics Conference and Exposition (APEC), 15-19 March 2015 2015, pp. 146-153, doi: 10.1109/APEC.2015.7104345.
- [32] J. Xiang, X. Ren, Y. Wang, and Y. Zhang, "Investigation of cascode structure GaN devices in ZCS region of LLC resonant converter," in 2017 IEEE Energy Conversion Congress and Exposition (ECCE), 1-5 Oct. 2017 2017, pp. 1374-1378, doi: 10.1109/ECCE.2017.8095950.
- [33] M. D. Seeman, S. R. Bahl, D. I. Anderson, and G. A. Shah, "Advantages of GaN in a high-voltage resonant LLC converter," in 2014 IEEE Applied Power Electronics Conference and Exposition - APEC 2014, 16-20 March 2014 2014, pp. 476-483, doi: 10.1109/APEC.2014.6803351.
- [34] L. Bing, L. Wenduo, L. Yan, F. C. Lee, and J. D. v. Wyk, "Optimal design methodology for LLC resonant converter," in Twenty-First Annual IEEE Applied Power Electronics Conference and Exposition, 2006. APEC '06., 19-23 March 2006 2006, p. 6 pp., doi: 10.1109/APEC.2006.1620590.
- [35] D. Huang, S. Ji, and F. C. Lee, "Matrix transformer for LLC resonant converters," in 2013 Twenty-Eighth Annual IEEE Applied Power Electronics Conference and Exposition (APEC), 17-21 March 2013 2013, pp. 2078-2083, doi: 10.1109/APEC.2013.6520582.
- [36] L. A. D. Ta, N. D. Dao, and D. Lee, "High-Efficiency Hybrid LLC Resonant Converter for On-Board Chargers of Plug-In Electric Vehicles," *IEEE Trans. Power Electron.*, vol. 35, no. 8, pp. 8324-8334, 2020, doi: 10.1109/TPEL.2020.2968084.
- [37] R. Beiranvand, B. Rashidian, M. R. Zolghadri, and S. M. H. Alavi, "Using LLC Resonant Converter for Designing Wide-Range Voltage Source," *IEEE Trans. Ind. Electron.*, vol. 58, no. 5, pp. 1746-1756, 2011, doi: 10.1109/TIE.2010.2052537.
- [38] Z. Liu, F. C. Lee, Q. Li, and Y. Yang, "Design of GaN-Based MHz Totem-Pole PFC Rectifier," *IEEE J. Emerg. Sel. Top. Power Electron.*, vol. 4, no. 3, pp. 799-807, 2016, doi: 10.1109/JESTPE.2016.2571299.
- [39] G. Cao, W. Dou, K. Sun, and Y. Wang, "Design Optimization of LLC Converter for Battery Charger with Wide Output Voltage Range," in 2018

- IEEE 27th International Symposium on Industrial Electronics (ISIE), 13-15 June 2018 2018, pp. 1182-1187, doi: 10.1109/ISIE.2018.8433642.
- [40] F. Musavi, M. Craciun, D. S. Gautam, W. Eberle, and W. G. Dunford, "An LLC Resonant DC–DC Converter for Wide Output Voltage Range Battery Charging Applications," *IEEE Trans. Power Electron.*, vol. 28, no. 12, pp. 5437-5445, 2013, doi: 10.1109/TPEL.2013.2241792.
- [41] X. D. Gumerá, A. Caberos, and S. Huang, "Design and Implementation of a High Efficiency Cost Effective EV Charger Using LLC Resonant Converter," in 2017 Asian Conference on Energy, Power and Transportation Electrification (ACEPT), 24-26 Oct. 2017 2017, pp. 1-6, doi: 10.1109/ACEPT.2017.8168618.
- [42] Y. Wei, Q. Luo, and A. Mantooth, "Overview of Modulation Strategies for LLC Resonant Converter," *IEEE Trans. Power Electron.*, vol. 35, no. 10, pp. 10423-10443, 2020, doi: 10.1109/TPEL.2020.2975392.
- [43] N. Kollipara, M. K. Kazimierczuk, A. Reatti, and F. Corti, "Phase Control and Power Optimization of LLC Converter," in 2019 IEEE International Symposium on Circuits and Systems (ISCAS), 26-29 May 2019 2019, pp. 1-5, doi: 10.1109/ISCAS.2019.8702652.
- [44] W. Liu, B. Wang, W. Yao, Z. Lu, and X. Xu, "Steady-state analysis of the phase shift modulated LLC resonant converter," in 2016 IEEE Energy Conversion Congress and Exposition (ECCE), 18-22 Sept. 2016 2016, pp. 1-5, doi: 10.1109/ECCE.2016.7855471.
- [45] H. Wu, T. Mu, X. Gao, and Y. Xing, "A Secondary-Side Phase-Shift-Controlled *LLC* Resonant Converter With Reduced Conduction Loss at Normal Operation for Hold-Up Time Compensation Application," *IEEE Trans. Power Electron.*, vol. 30, no. 10, pp. 5352-5357, 2015, doi: 10.1109/TPEL.2015.2418786.
- [46] X. Sun, X. Li, Y. Shen, B. Wang, and X. Guo, "Dual-Bridge LLC Resonant Converter With Fixed-Frequency PWM Control for Wide Input Applications," *IEEE Trans. Power Electron.*, vol. 32, no. 1, pp. 69-80, 2017, doi: 10.1109/TPEL.2016.2530748.
- [47] K. J. Chen et al., "GaN-on-Si Power Technology: Devices and Applications," *IEEE Transactions on Electron Devices*, vol. 64, no. 3, pp. 779-795, 2017, doi: 10.1109/TED.2017.2657579.
- [48] J. Millán, P. Godignon, X. Perpiñà, A. Pérez-Tomás, and J. Rebollo, "A Survey of Wide Bandgap Power Semiconductor Devices," *IEEE Trans. Power Electron.*, vol. 29, no. 5, pp. 2155-2163, 2014, doi: 10.1109/TPEL.2013.2268900.
- [49] P. Roussel, "SiC market and industry update," *Int. SiC Power Electron. Appl. Workshop*, 2011.
- [50] J. Jee-hoon and K. Joong-gi, "Theoretical analysis and optimal design of LLC resonant converter," in 2007 European Conference on Power Electronics and Applications, 2-5 Sept. 2007 2007, pp. 1-10, doi: 10.1109/EPE.2007.4417639.
- [51] "LMG341xR070 600-V 70-mΩ GaN with Integrated Driver and Protection datasheet (Rev. F)," may 2020 ed, 2020.
- [52] "Datasheet IPB60R070CFD7," 5-2019 ed, 2019.

## BIOGRAPHY

<b>NAME</b>	Jie Gan
<b>DATE OF BIRTH</b>	August 25, 1992
<b>PLACE OF BIRTH</b>	China
<b>ADDRESS</b>	No.101, Daxuedonglu Road, Nanning City, Guangxi Province, China
<b>EDUCATION</b>	2015 Bachelor degree of Engineering, Chengdu University of Information Technology, China 2022 Master degree of Electrical and Computer Engineering, Mahasarakham University, Thailand

